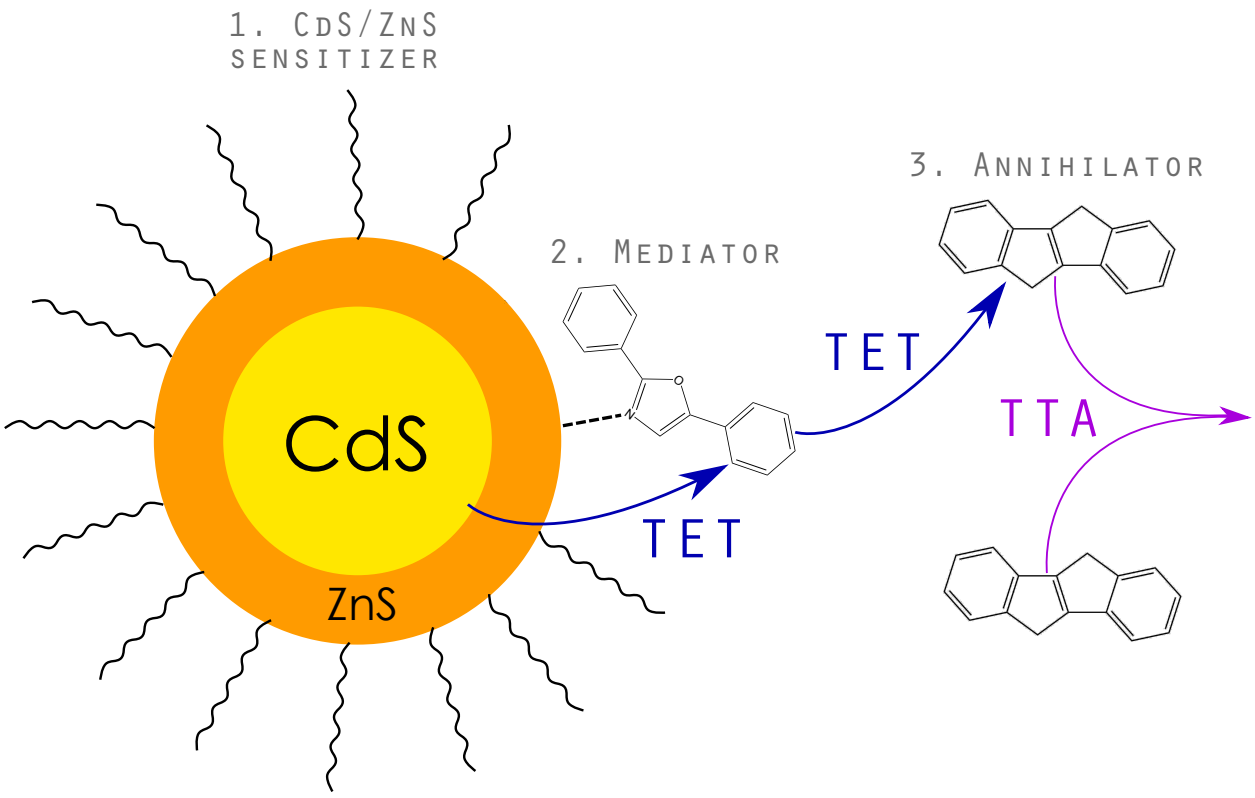
CHALMERS
UNIVERSITY OF TECHNOLOGY



Towards visible-to-UV photon upconversion

A study of annihilator candidates for upconversion through core-shell nanoparticle sensitized triplet-triplet annihilation

Master's Thesis in Nanotechnology

AXEL OLESUND

Department of Chemistry and Chemical Engineering
CHALMERS UNIVERSITY OF TECHNOLOGY
Gothenburg, Sweden 2018

Towards visible-to-UV photon upconversion

A study of annihilator candidates for upconversion through core-shell nanoparticle sensitized triplet-triplet annihilation

AXEL OLESUND



CHALMERS
UNIVERSITY OF TECHNOLOGY

Department of Chemistry and Chemical Engineering
Chalmers University of Technology
Gothenburg, Sweden 2018

Towards visible-to-UV photon upconversion
A study of annihilator candidates for upconversion through core-shell nanoparticle sensitized triplet-triplet annihilation
AXEL OLESUND

© AXEL OLESUND, 2018.

Supervisor: Fredrik Edhborg, Department of Chemistry and Chemical Engineering
Examiner: Bo Albinsson, Department of Chemistry and Chemical Engineering

Department of Chemistry and Chemical Engineering
Chalmers University of Technology
SE-412 96 Gothenburg
Telephone +46 31 772 1000

Cover: Visualization of the mechanisms involved for transferring energy between participating compounds in sensitized triplet-triplet annihilation.

Typeset in LaTeX
Gothenburg, Sweden 2018

Towards visible-to-UV photon upconversion
A study of annihilator candidates for upconversion through core-shell nanoparticle sensitized triplet-triplet annihilation
AXEL OLESUND
Department of Chemistry and Chemical Engineering
Chalmers University of Technology

Abstract

Efficient harvesting of solar energy may provide the key to solving current global energy issues. Today's solar technologies have some limitations as they only exploit parts of the solar spectra efficiently. Upconversion (UC) is a promising concept where lower energy photons are transformed into photons of higher energy, and provides a pathway to more efficient use of solar energy. In this study, visible light is upconverted into the ultra-violet part of the spectra by employing the triplet-triplet annihilation (TTA) mechanism. This is realized by using three interacting compounds. The sensitizer, which is responsible for light absorption, is a core-shell type nanoparticle and consists of a cadmium sulfide (CdS) core and a zinc sulfide (ZnS) shell. These nanoparticles have been synthesized using the hot injection method and characterized by means of absorption and emission spectroscopy. Eight different molecules are investigated in the role of annihilator, which undergoes TTA and emits the upconverted photons. Two compounds are investigated in the role of mediator, which facilitates energy transfer from sensitizer to annihilator. Spectroscopic methods have been used when characterizing and evaluating these compounds.

This study confirms that 2,5-diphenyloxazole (PPO) may be utilized both as mediator and annihilator. In addition, 2,5-diphenyl-1,3,4-oxadiazole (PPD) has emerged as a potential mediator compound. The triplet energy transfer from sensitizer to mediator seems to be slightly more efficient when PPD is utilized. However, the resulting UC emission from PPO is higher if PPO is also used as mediator, possibly indicating that PPO take on the role of mediator also in the presence of PPD. The seven compounds that hadn't been tested as annihilators previously did not produce any UC emission. Considering suboptimal sensitizer quality and UC experimental setup, this result may not solely stem from these compounds being unable to undergo TTA. To get a full understanding of why so few compounds has worked, further experiments using the functioning annihilator (PPO) as well as non-functioning annihilators must be performed. Enhancing the sensitizer quality and optimizing the experimental setup is also vital in order to increase understanding of this very complex mechanism.

Keywords: solar energy, upconversion, triplet-triplet annihilation, CdS/ZnS nanoparticles, spectroscopy, mediator, annihilator

Acknowledgements

My sincerest gratitude goes out to my supervisor Fredrik Edhborg, who has supplied tremendous amounts of time, knowledge and curiosity during the proceedings of this study. I would also like to thank Professor Bo Albinsson who suggested the project, and who has gently steered it in the right direction. Big thanks also go out to everyone in the *Unconventional solar energy group* at Chalmers, with a special mention of Victor Gray who has provided invaluable expertise during the nanoparticle synthesis.
I would also like to thank all my fellow classmates at Chalmers for countless hours of interesting discussions and laughter, my parents for their unwavering love and support, and lastly my girlfriend Lisa, who constantly brings new perspectives on things and never fails to cheer me up when most needed.

Axel Olesund, Gothenburg, June 2018

Contents

List of Figures **xi**

List of Tables **xv**

List of Acronyms **xvii**

1 Introduction **1**
1.1 Purpose . . . 2
1.2 Limitations . . . 3
1.3 Specification of question formulation . . . 3

2 Photon upconversion **5**
2.1 Light and matter in the quantum regime . . . 5
2.1.1 Electronic states . . . 5
2.1.2 Photoinduced processes . . . 7
2.1.3 Quantum yield, Stokes shift, and quenching . . . 8
2.2 Upconversion . . . 9
2.2.1 Energy transfer mechanisms . . . 9
2.2.1.1 Förster resonance energy transfer . . . 9
2.2.1.2 Dexter energy transfer . . . 10
2.2.2 Triplet-triplet annihilation . . . 11
2.2.3 sTTA-UC efficiency . . . 13
2.3 Sensitizers and annihilators for upconversion . . . 14
2.3.1 CdS/ZnS core-shell nanoparticles . . . 15
2.3.2 Annihilator candidates . . . 16

3 Methods **19**
3.1 Spectroscopic methods . . . 19
3.1.1 Steady-state absorption spectroscopy . . . 19
3.1.2 Emission spectroscopy . . . 20
3.1.2.1 Time-resolved emission spectroscopy . . . 21
3.1.3 Upconversion measurements . . . 21
3.2 CdS/ZnS core-shell NP synthesis . . . 22
3.2.1 CdS core synthesis . . . 22
3.2.2 ZnS shell growth . . . 23
3.2.3 Mediator/ligand exchange and UC measurements . . . 24

4 Results and Discussion **27**

4.1 Synthesis of CdS/ZnS core-shell NPs 27
4.1.1 Initial characterization of CdS/ZnS NPs 27
4.1.2 Synthesis considerations and optimization 30
4.2 Annihilator characterization 31
4.3 Ligand/mediator exchange investigation 33
4.3.1 Measurements on quenching efficiency 33
4.3.2 Quantifying the number of surface bound mediators 35
4.4 Upconversion measurements 36
4.4.1 Effect on UC by change of mediator 36
4.4.2 Novel annihilator UC measurements 38
4.4.3 Future directions in vis-to-UV UC research 39

5 Conclusion **41**
5.1 Future outlook 41

Bibliography **43**

A Appendix 1 **I**
A.1 Calculation: Amount of $Zn(DTTC)_2$ needed for ZnS shell growth . . I

List of Figures

2.1 A Jablonski diagram describing different transitions between states within a molecule. S_i describes the singlet energy levels, T_i the triplet energy levels, VR is *vibrational relaxation*, ISC is *intersystem crossing*, and IC is *internal conversion*. Colored arrows depict events resulting from photon absorption or emission. Thick, black horizontal lines depict the electronic energy levels while thin horizontal lines are vibrational energy levels. 7

2.2 Intermolecular energy transfer mechanisms. In all three cases the energy from an excited donor is transferred to an acceptor, which is excited following the transfer. The short-range Dexter energy transfer involves the actual swopping of electrons between interacting species. Excited states are marked with *, whilst numeric superscripts denote spin multiplicity of singlet and triplet states respectively. 10

2.3 The ideal triplet-triplet annihilation mechanism. S and A denotes sensitizer and annihilator, respectively, while superscripts denote spin multiplicity. Photon absorption by the sensitizer is followed by intersystem crossing (ISC) to its triplet excited state. Subsequent triplet energy transfer (TET) populates the annihilator triplet excited states, which can then perform triplet-triplet annihilation as they meet. The singlet excited annihilator then emits one upconverted photon. 12

2.4 Energy transfer schematic for the usage of a mediator. The mediator, here represented by 2,5-diphenyloxazole (PPO), binds to a zinc site of the CdS/ZnS NP via a nitrogen atom. This bond enables TET from sensitizer to mediator. Subsequent TET from mediator to an annihilator in solution is followed by TTA between two annihilator molecules. For a more detailed description of the energetic relationships, see Figure 2.3. 16

2.5 The eight different annihilator candidates. The energy values have been calculated using Density Functional Theory and give indications on each compounds potential for UC. The value of greatest importance is that in the right-hand side column, which must be positive in order for TTA to happen. 17

3.1 The experimental setup for absorption measurements. The monochromator selects one wavelength at the time and the sample detector measures the intensity of non-absorbed light. Sweeping over a range of wavelengths in the monochromator creates an absorption spectrum of the sample. 19

3.2 Normalized absorption and emission spectra for the common fluorophore 9,10-diphenylanthracene (DPA). 20
3.3 The experimental setup for emission measurements. The difference from an absorption measurement setup is that the excitation monochromator typically is fixed at one specified wavelength, and that the sample detector measures the emission from the sample. A second monochromator selects one wavelength at the time that is allowed to pass, and by sweeping over a range of wavelengths an emission spectrum may be obtained. 21
3.4 The experimental setup for UC measurements. Two lenses are employed to focus as much of the diverging light from the LED as possible. The power supply drives the lamp, and can be used to alter the light intensity from the LED. 22
3.5 Synthesis scheme for the production of CdS/ZnS core-shell NPs. The CdS cores are synthesized by addition of sulfur powder at high temperature. Subsequent shell growth is done by addition of the zinc precursor $Zn(DTTC)_2$ and stirring at ∼185 ℃. The shell growth procedure was repeated four times. The wiggly lines on the surface are ligands of oleic acid. 23

4.1 Image of the CdS/ZnS NPs obtained through TEM. The NP size is generally a bit larger than the expected 4.5 nm in diameter, and the shapes are slightly non-uniform. 28
4.2 Absorption and emission of the batch no. 5 NPs during the different steps of shell growth. An immediate red-shift (from 395 to 442 nm for the absorption) is observed following the growth of the first ML. Growth of additional MLs effectively eliminates the emissive trap states that are seen in the range of 450 to 700 nm for 0ML to 2ML. Initially the NP emission is quenched as ZnS MLs are added, but as the 4th ZnS ML is added a severe increase of the emission is evident. 29
4.3 Time-resolved emission spectroscopy measurement on CdS/ZnS NPs. The black solid line is a best fit using three exponential terms. The measurement was done using 377 nm excitation light. 30
4.4 A snapshot of the CdS/ZnS mixture during the synthesis of batch no. 5. Its vivid yellow color is a result of strong absorption of light in the blue and UV part of the spectrum. To the right one can see the thermometer stick that is inserted through a septum on one of the bottlenecks into the reaction mixture itself. 31
4.5 Steady-state absorption and emission spectra for the eight annihilator candidates. 32
4.6 A series of absorption and emission measurements with PPO as the mediator. The green and light-blue spectra are from measurements on the same sample, with the ”1week” notion indicating that the light-blue measurement was performed one week after the green one. The same goes for the blue/purple spectra. 33

4.7 A series of absorption and emission measurements with PPD as the mediator. The NP emission is quenched by about 50% as PPD binds to the surface. 34
4.8 Absorption of NP/PPO systems of three different ratios, together with the absorption of pure NPs. The PPO feature is only clearly visible for the sample with a 1:1000 NP:PPO ratio. Note that these samples have *not* been cleaned following the addition of PPO. 35
4.9 The recorded emission from a sample where PPO is utilized as both mediator and annihilator. Upconverted emission from PPO is clearly distinguishable under 405 nm excitation light. The UC emission is centered around 355 nm which is the emission maxima for PPO in hexane (blue solid line). 37
4.10 Upconverted emission from two different samples under 405 nm excitation light: one with PPO as mediator (red line) and one with PPD as mediator (blue line). The green line is the blue spectra normalized with respect to the 570 nm peak to match that of the red one. Both samples utilized PPO as annihilator. 37
4.11 UC measurements on three different samples, using DPB and DPH as annihilators. DPH emits at too low energies to actually enable UC. If DPB would have been emitting, this should present itself in the form of emission around 360 nm. 39

List of Tables

4.1 Absorption and emission characteristics of the five synthesis efforts. Two batches failed completely and did not return any detectable particles at all. Batch 3 went awry during the ZnS shell growth, and the very last batch was discarded as a result of issues in the final purification step. 27
4.2 Summary of the results from the UC measurements. PPO is the only compound that was successfully utilized in the role of annihilator, producing upconverted emission in the 340 nm to 370 nm wavelength range. 38

List of Acronyms

BPB - 1,4-bis(phenylethynyl)benzene
CdS - Cadmium sulfide
CdSe - Cadmium selenide
DET - Dexter energy transfer
DPA - 9,10-diphenylanthracene
DPB - 1,4-diphenyl-1,3-butadiene
DPF - 2,5-diphenylfuran
DPH - 1,4-diphenyl-1,3,5-hexatriene
FRET - Förster resonance energy transfer
HOMO - Highest occupied molecular orbital
I2 - 5,10-dihydro-indeno[2,1-a]indene
IC - Internal conversion
IR - Infra-red
IRF - Instrument response function
ISC - Intersystem crossing
LED - Light-emitting diode
LUMO - Lowest unoccupied molecular orbital
ML - Monolayer
NP - Nanoparticle
ODE - 1-octadecene
PPD - 2,5-diphenyl-1,3,4-oxadiazole
PPO - 2,5-diphenyloxazole
QY - Quantum yield
SET - Singlet energy transfer
sTTA-UC - Sensitized triplet-triplet annihilation upconversion
TCSPC - Time correlated single photon counting
TEM - Transmission electron microscopy
TET - Triplet energy transfer
TTA - Triplet-triplet annihilation
TS - Trans-stilbene
UC - Upconversion
UV - Ultra-violet
vis-to-UV - visible to ultra-violet
$Zn(DTTC)_2$ - Zinc diethyldithiocarbamate
ZnS - Zinc sulfide

1
Introduction

In a time where climate change poses an ever increasing threat against humanity, the search for renewable energy sources is of crucial importance. Luckily, our closest star provides the Earth with copious amounts of energy each day, making the harvesting of solar energy a very promising prospect. In fact, the world's total energy consumption could be covered if only 0,01% of the solar energy was harvested.[1] However, there are several challenges associated with this, including such things as cost-efficiency, large-scale production and solar conversion efficiency.

One major issue is the fact that the whole solar spectrum can't be absorbed at once. Depending on what material is utilized, only energies above a threshold value specific to this material will be absorbed. Additionally, the excess energy of photons with energies above this value will be wasted. By combining different semiconducting materials in the cells the efficiency of solar cells has made great progress[2] and many different techniques that could overcome some of the previously mentioned issues are currently being developed. However, instead of trying to expand the absorptive properties of e.g. solar cells, one could manipulate the incoming photons. The concept of *upconversion* (UC), which is the creation of one high-energy photon from two low-energy photons, has in later years reemerged as a promising way of increasing solar efficiency after gaining some recognition earlier in the 1970's.[3] Some success has been achieved in upconverting green light to blue light, but big challenges remain in optimizing the process as the highest achieved UC quantum yield currently lies at 38%[4] (which should be considered in relation to the upper theoretical UC quantum yield limit of 50%[5]).

There are intense research in near-IR-to-visible UC and, as previously mentioned, also in UC between different wavelengths of visible light. Another promising way of utilizing UC is to take visible light of rather high energy (e.g. blue light) and create high energy ultra-violet (UV) light. UV light is scarce in the solar irradiation that reaches earth due to the ozone layer absorbing most of it. This is of course a good thing as an excess of UV light can be harmful to life, but for certain photochemical reactions, such as water-splitting, it is of great importance. In this process water is divided into oxygen, O_2, and hydrogen gas, H_2.[6] H_2 has for many years been considered a potential fuel, especially for the transport sector,[7] but there have been several limiting factors to the development of this technique. One of the main concerns regarding hydrogen as a fuel is the difficulties in storage, but also problem arise from the production phase. Current production of hydrogen is heavily dependent of the use of fossil fuels,[8] thus there is an urgent need for alternative production methods.

Using water splitting for hydrogen production holds great promise as the water splitting stoichiometric quantum yield under 270 nm (i.e. UV) light has been shown

to be as high as 56%.[9] In order to even consider approaching such high levels of water-splitting quantum yield using sunlight, efficient UC of visible light to UV light (vis-to-UV) is a requirement. Unfortunately, this is very much an area of research which hasn't attained the attention it deserves. The first demonstration of vis-to-UV UC came in the late 60's when Parker and Joyce observed UV emission in a solution of benzophenone and naphthalene,[10] but it gained no real interest until much later. The theories behind this phenomenon wasn't thoroughly developed at this time but in 2004 a similar study, utilizing partly the same compounds, gave a clearer explanation of the results.[11] Much have happened since then, but compared to UC into the visible range the interest has been fairly low.

The concept of UC is quite straight-forward, but the underlying mechanisms prove to be more complicated. There are several mechanisms that can achieve UC, such as two photon absorption, but the most promising mechanism for solar applications is called *triplet-triplet annihilation* (TTA). In contrast to two photon absorption, the TTA process works under non-coherent low intensity light, which means that sunlight can be utilized as the light source.[12] For this process one must find a compound which fulfill a set of certain criteria, such as that it must be fluorescent. For the vis-to-UV UC this compound, generally referred to as the *annihilator*, have to fluoresce within the UV spectrum. Apart from this a suitable *sensitizer* must be chosen, and this compound is responsible for the initial absorption of photons. This absorption must take place at a higher wavelength than that of the resulting fluorescence from the annihilator in order to achieve actual UC. The complete process, usually referred to as *sensitized triplet-triplet annihilation upconversion* (sTTA-UC), may or may not involve even more compounds. This study will for instance make use of a so-called *mediator*, a compound which will facilitate the energy transfer between sensitizer and annihilator.

Different sensitizers and annihilators have previously been utilized, and a first reported vis-to-UV UC quantum yield (QY) of 0,58% was presented in 2009 after employing 2,3-butanedione (biacetyl) as the sensitizer and 2,5-diphenyloxazole (PPO) as the annihilator. Lately, great progress has however been made in terms of increased UC QY by utilization of different sensitizer-annihilator pairs, surpassing 1% in 2014[13] and reaching as high as 1,95% in 2016.[14] This is, at the best of my knowledge, the highest achieved UC QY by utilizing an organic sensitizer for vis-to-UV UC. Recent efforts, which employs nanoparticles as the sensitizer with a cadmium sulfide (CdS) core and a zinc sulfide (ZnS) shell, has however surpassed the organic sensitizers and produced an impressive UC QY of 2,6%.[15] Vis-to-UV UC has also been demonstrated in solid films, again using PPO as annihilator.[16] It is however obvious that there is a lot left to do within this field, and there are many gaps in knowledge that needs to be filled in order to create more efficient systems. The reasons behind why vis-to-UV UC is so hard to achieve are partly unknown, and this study aims to provide answers to some important questions related to this.

1.1 Purpose

The main purpose of this thesis is to investigate a number of potential candidates for the role of annihilators in the vis-to-UV sTTA-UC process, thus developing a better

understanding of the underlying mechanisms. The results of this thesis will hopefully provide valuable input for the research focusing on understanding the limitations of vis-to-UV sTTA-UC, create knowledge in the area and in the long run help creating more efficient methods for harvesting solar energy.

1.2 Limitations

Many different aspects could be covered by a thesis like this one. This thesis will however, from a researching point of view, focus primarily on the annihilators as these are the new thing that will be tested. The synthesis of CdS/ZnS nanoparticles has been previously utilized for vis-to-UV UC[15] and this study do not strive to optimize the synthesis or the characteristics of the nanoparticles as such. Neither will it investigate the use of possible different mediators in the process, instead the previously used mediator 2,5-diphenyloxazole (PPO) and its close relative 2,5-diphenyl-1,3,4-oxadiazole (PPD) are the two that will be utilized and characterized. Other aspects that won't be covered are the environmental impact and toxicity of cadmium (Cd), which is an important component of the nanoparticles.

1.3 Specification of question formulation

A few specific tasks will be performed during this study in order to answer the following question:

- Which mediator, PPO or PPD, is most efficient for the vis-to-UV UC?
- How well do the respective mediator bind to the ZnS-shell of the nanoparticles?
- What are the spectroscopic characteristics of the sensitizer, mediators and annihilators?
- What UC QY can be achieved with the different annihilators?
- Which are the limiting factors, or steps, for the sTTA-UC when using the different annihilators?

2

Photon upconversion

The following section aims to present some fundamental theories necessary in order to fully appreciate the results presented later on. Basic theories regarding the nature of light, matter and how they can interact with each other is first presented before the mechanisms which are important for the UC as such are explained.

2.1 Light and matter in the quantum regime

Light consists of two oscillating fields, one electric and one magnetic field. These are perpendicular to each other and also to the propagation direction of the light. Light is hence often referred to as *electro-magnetic radiation*. All light have a frequency (ν) and a wavelength (λ), where the latter is defined as the distance between two maxima of one of the oscillating fields. Light can also be considered to be made up of discrete particles called photons. This wave-particle duality exists also for macroscopic particles but the wave properties are usually not detectable due to extremely short wavelengths. Visible light has wavelengths ranging from about 400 to 700 nm and because of this both wave and particle properties are readily detectable. This is also true for ultra-violet (UV) light (λ = 10 to 400 nm) and infra-red (IR) light (λ = 0.7 to 1000 μm).

The energy (E) of one photon is calculated from the frequency of the electromagnetic wave, *Planck's constant* ($h = 6.626\times10^{34}$ Js), and the speed of light in vacuum ($c = 2.998\times10^{8}$ ms^{-1}) using Equation 2.1

$$E = h\nu = \frac{hc}{\lambda} \tag{2.1}$$

As can be understood from this equation, a shorter wavelength results in light of higher energy. Because of this, UV light with wavelengths shorter than 400 nm is higher in energy than visible light.

2.1.1 Electronic states

To understand how light may interact with matter one must have a good understanding of electrons. Even though electrons are not the only fundamental component of the atom (positive protons and neutral neutrons make up the atomic nucleus) they are indeed of greatest interest for the relevant concepts of this thesis. As the negative electron is very small in size one must go to quantum mechanics in order to give it a thorough description. One important property that differs from macroscopic objects is that the electron, when part of an atom or molecule, have *discrete*

energy levels. The electron can thus only exist in the electronic states corresponding to these energy levels. The electronic quantum states are closely related to what is called the *quantum numbers*, which are divided into four groups. The principal quantum number (n = 1, 2, 3, ...) directly relates to the energy of the electron and are often referred to as the electronic *shells* of the atom. The innermost shell (usually referred to as the "K" shell) has $n = 1$ and can hold up to two electrons. The next shell (the "L" shell) will hold up to eight electrons with $n = 2$. The shell model is however quite a simplification but can be expanded by introducing the next quantum number, called the azimuthal quantum number. It is denoted by l and can take the values $l = 0, 1, 2, ..., n\text{-}1$. It describes the angular momentum of the atomic orbitals which holds the electrons. For $n = 2$ one gets $l = 0$ (usually referred to as the s orbital) and $l = 1$ (the p orbitals). The third quantum number, the magnetic quantum number (m_l), then describes the different directions an atomic orbital of specified n and l can take. It can take the values of $m_l = 0, \pm1, ..., \pm l$, and for $l = 1$ one gets three values for m_l corresponding to the p_x, p_y, and p_z orbitals. The last quantum number, m_s, is the spin magnetic quantum number and describes the intrinsic angular momentum, s, of the particle itself. The spin magnetic quantum number can take the values of $m_s = -s, -s+1, ..., s\text{-}1, s$. For the electron $s = \frac{1}{2}$, and thus this quantum number can only take two values, $m_s = \pm\frac{1}{2}$. This is usually referred to as spin up or spin down electrons.

The *Pauli exclusion principle* states that two fermions (electrons for instance) cannot occupy the same quantum state. Because of this, no electron can have the same set of quantum numbers as another electron in the same system. An atomic orbital will thus hold up to two electrons, one with spin up and one with spin down. The *total* spin angular momentum of these two electrons, S, can take the values of Equation 2.2

$$S = s_1 + s_2, s_1 + s_2 - 1, ..., |s_1 - s_2| \tag{2.2}$$

where s_i is the intrinsic angular momentum s of particle i. For a system consisting of two electrons one get two possible outcomes: $S = 0$ or $S = 1$. Further, the *spin multiplicity* of a state, $M = 2S + 1$, specifies the number of directions the spin component of a state can have. For $S = 0$ one gets $M = 1$, which corresponds to a *singlet* state. Most systems have singlet states as their ground state and they consist of paired electrons, one spin up and one spin down in each orbital. If $S = 1$ however, $M = 3$ which means it has a *triplet* state. The total spin magnetic quantum number, $M_s = S, S-1, ..., -S$, of such a system can take on the values -1, 0, and 1 and thus have three different orientations. Triplet ground states are very rare since the Pauli exclusion principle states that electrons in the same orbital must be paired. The triplet ground state do however appear in molecular oxygen.[17] This is because oxygen has some degenerate molecular orbitals which are filled with one *unpaired* electron, and these will have the same spin according to Hund's rule. Even higher spin multiplicities are possible for many-electron systems, such as molecules. One can e.g. have *quintet* states for systems where $S = 2$.

2.1.2 Photoinduced processes

So far we have talked about what different states there is within a system, such as a molecule, but it gets really interesting when one starts looking at how energy is transferred between different states. In Figure 2.1 a so called *Jablonski diagram* is presented, and it is used to illustrate different kinds of transitions between states in a system. The thick, colored arrows indicates excitation or deexcitation as a result of photon absorption or emission. *Fluorescence* is the radiative emission of a photon from an excited singlet state of the system while *phosphorescence* is radiative emission from an excited triplet state. *Internal conversion* (IC) followed by *vibrational relaxation* form the pathway for non-radiative transfer between states of the same spin multiplicity, such as between two singlet states. This process is generally very fast, and as a result the spontaneous fluorescence of a compound typically comes from the lowest excited singlet state (denoted S_1 in Figure 2.1).

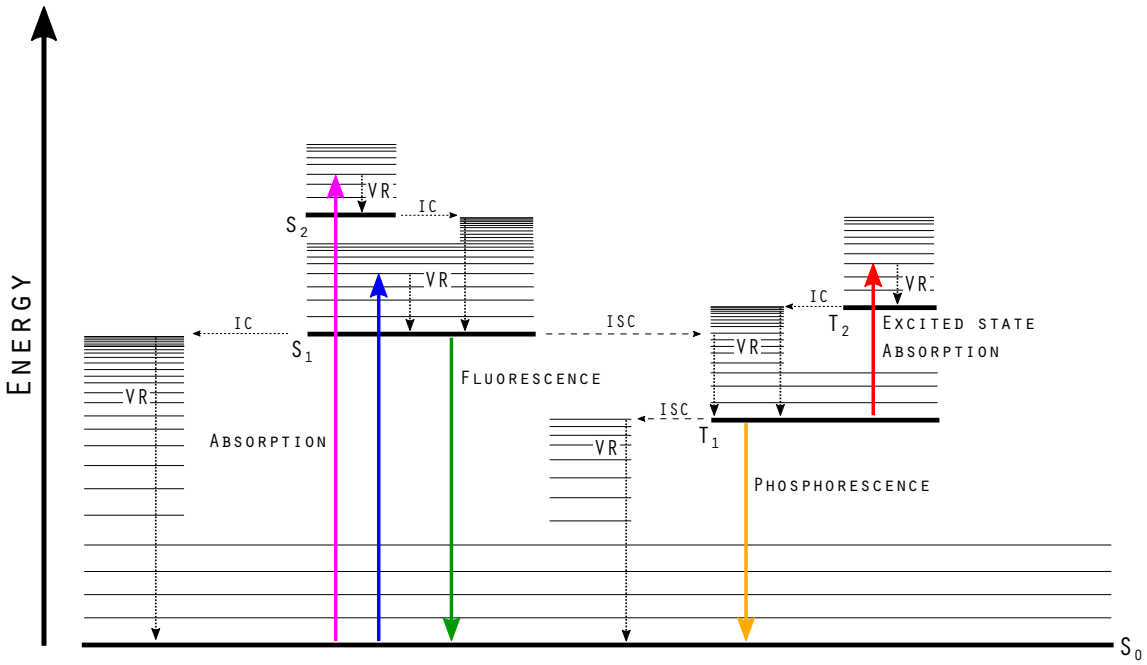


FIGURE 2.1: A Jablonski diagram describing different transitions between states within a molecule. S_i describes the singlet energy levels, T_i the triplet energy levels, VR is *vibrational relaxation*, ISC is *intersystem crossing*, and IC is *internal conversion*. Colored arrows depict events resulting from photon absorption or emission. Thick, black horizontal lines depict the electronic energy levels while thin horizontal lines are vibrational energy levels.

To reach the excited triplet state (denoted T_1 in Figure 2.1) the electron must undergo *intersystem crossing* (ISC). This is a non-radiative process which lets the molecule move between states of different spin multiplicity, and involves a change in electron spin. This is classically a "forbidden" spin transition as the ground state electron and excited state electron are no longer paired, thus the formation of a triplet excited state is less probable than its singlet counterpart. However, in some heavier molecules, such as those containing iodine or bromine, ISC and subsequent phosphorescence is more commonly found.[18] As the relaxation from T_1

to S_0 is also a spin-forbidden transition, the rate constants for phosphorescence are several magnitudes smaller than those of fluorescence. In practice this leads to that phosphorescence is slower and lower in intensity, and some phosphorescent materials can because of this emit light for up to a few hours following illumination. As T_1 always lies lower in energy than S_1 (see Figure 2.1) phosphorescence takes place at longer wavelengths than fluorescence. *Excited state absorption* is used to excite already excited molecules to the next excited state (e.g. from T_1 to T_2) and is commonly used to measure e.g. excited state lifetimes or to trace intermediate states in a photophysical process.

2.1.3 Quantum yield, Stokes shift, and quenching

There are a few more terms that need presentation before moving on to the UC mechanisms. The *quantum yield* (QY) describes how many times a specific event occurs per absorbed photon, and may be used as a measurement for several different events. In photochemistry it is perhaps most commonly used to measure fluorescence QY, Φ_f, i.e. the ratio between the number of emitted photons and absorbed photons. Equation 2.3 presents a general expression of QY evaluation for some process i.

$$\Phi_i = \frac{k_i}{\sum_j k_j} \tag{2.3}$$

k_i is the rate of process i and k_j is the rate of process j. In the fluorescence case there are generally only two kinds of processes that are of interest, radiative relaxation (with its corresponding rate constant k_r) and non-radiative relaxation (with rate constant k_{nr}). Φ_f is then just the ratio between k_r and the sum of k_r and k_{nr}. Later on we will see that some cases are a bit more complex.

Since photon absorption is usually followed by vibrational relaxation (see Figure 2.1) it makes sense that subsequent fluorescence occur at a longer wavelength than the absorption due to energy being lost during VR. This difference in energy between absorbed and emitted photons is called *Stokes shift*, and is commonly noted as the energy difference between the absorption and emission maxima. An important note is that this has nothing to do with the *intensity* of the fluorescence but only with the wavelength of participating photons. In the case of UC, where the emitted photons have higher energy than the initially absorbed photons, one usually talks about it as *anti-Stokes shift*. There are however other processes that may affect fluorescence intensity negatively which leads to lower Φ_f. The term for a process that leads to decreased fluorescence is *quenching*, and may depend on a number of different things. One example of quenching is ISC, and another one is the re-absorption of emitted light. This can occur if the Stokes shift is quite small, thus creating a spectral overlap between the absorption and emission spectra. Quenching can also appear because of the presence of oxygen. Because of oxygen having a triplet ground state of quite low energy it can effectively quench the triplet excited states of surrounding compounds.[19]

2.2 Upconversion

The UC concept has been introduced in Section 1 but the creation of one high energy photon from two low energy photons is far from intuitive. To fully understand the UC mechanisms one must first understand how energy can be transferred not only within molecules but also between different molecules. Of specific interest is the intermolecular energy transfer between one excited molecule and one in its ground state.

2.2.1 Energy transfer mechanisms

Of interest in this thesis are two types of energy transfer, namely *singlet energy transfer* (SET) and *triplet energy transfer* (TET). Within SET there are two distinct transfer mechanisms that are particularly interesting, *Förster resonance energy transfer* (FRET) and *Dexter energy transfer* (DET).

2.2.1.1 Förster resonance energy transfer

FRET is a non-radiative energy transfer mechanism that takes place between an excited donor molecule and an acceptor molecule in its ground state. It is dependent on the normalized spectral overlap between the donor emission and the acceptor absorption, the relative orientation between transition moments, and the distance between the molecules. It should however be noted that there is no actual emission and absorption of a photon involved in this energy transfer, the energy transfer is instead a result of dipole-dipole interactions between the electronic states of the molecules,[18] see Figure 2.2. The efficiency of FRET is usually expressed in terms of the so called *Förster distance*, R_0, which is a measure of molecular orientation and of how extensive the spectral overlap between interacting molecules is. R_0 is calculated in accordance with Equation 2.4

$$R_0 = 0.211(\kappa^2 n^{-4} \Phi_D \int_0^\infty F_D(\lambda)\epsilon_A(\lambda)\lambda^4 d\lambda)^{1/6} \tag{2.4}$$

κ^2 is a factor describing the orientation between donor and acceptor transition moments, n is the refractive index, Φ_D is the donor fluorescence QY, F_D is the normalized fluorescence spectrum of the donor, ϵ_A is the molar absorptivity of the acceptor, and λ is the wavelength. The integral in R_0 is called the *spectral overlap integral* and calculates the area of the previously mentioned spectral overlap. The resulting efficiency, η_{FRET}, of the energy transfer is then calculated with Equation 2.5

$$\eta_{FRET} = \frac{R_0^6}{R_0^6 + r^6} \tag{2.5}$$

where r is the intermolecular distance between the two interacting molecules. FRET is thus proportional to r^{-6}, but since R_0 is generally 30 to 60 Å the efficiency can be quite high even for relatively large donor-acceptor separations.[18]

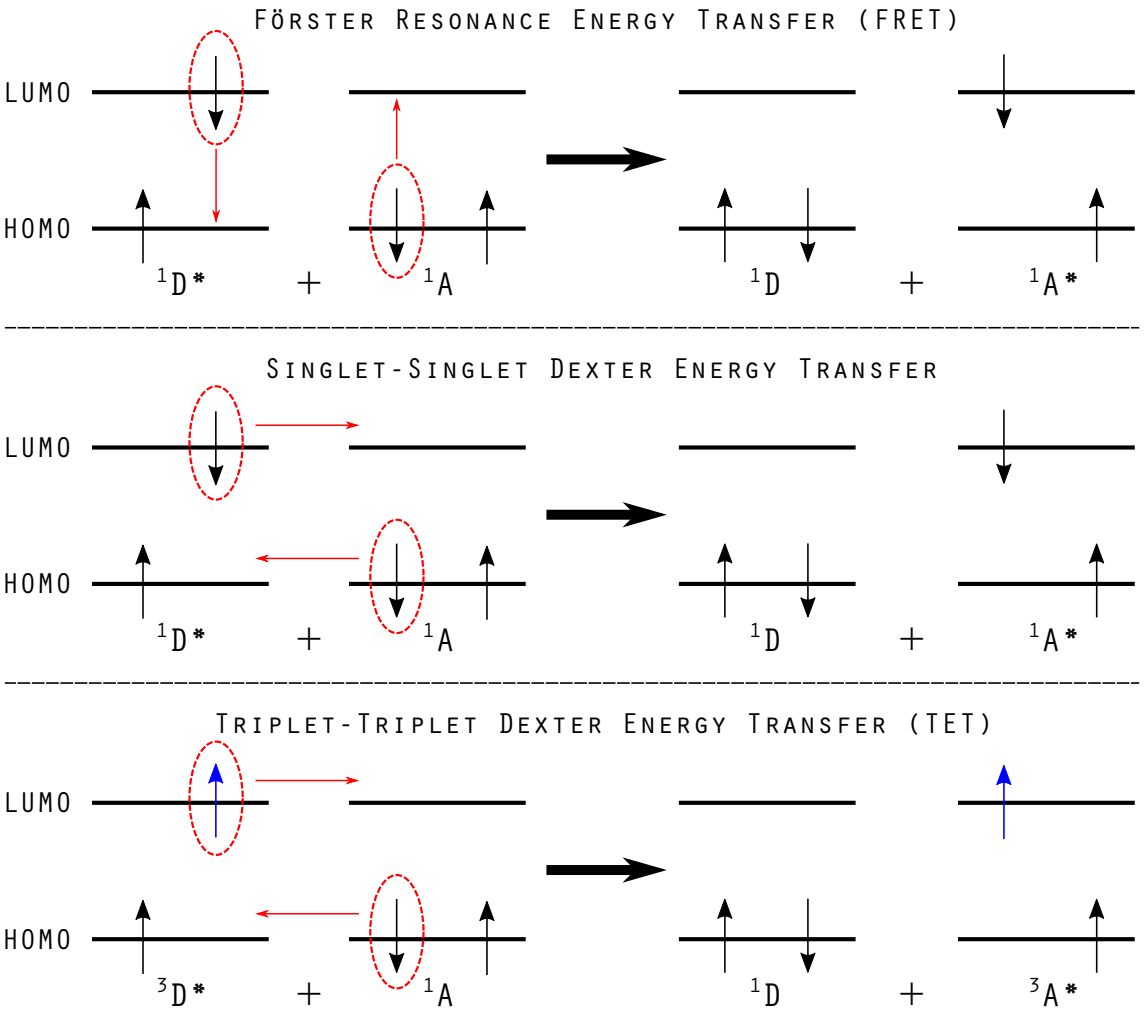


Figure 2.2: Intermolecular energy transfer mechanisms. In all three cases the energy from an excited donor is transferred to an acceptor, which is excited following the transfer. The short-range Dexter energy transfer involves the actual swopping of electrons between interacting species. Excited states are marked with *, whilst numeric superscripts denote spin multiplicity of singlet and triplet states respectively.

2.2.1.2 Dexter energy transfer

In contrast to FRET, the Dexter energy transfer mechanism involves an actual electron exchange between the two interacting species. One important difference from FRET is also that the Dexter mechanism is available both for SET and TET, which is illustrated in Figure 2.2 alongside the FRET mechanism. It involves the simultaneous transfer of two electrons between the *lowest unoccupied molecular orbitals* (LUMO) and *highest occupied molecular orbitals* (HOMO) of the interacting molecules. For this to happen there must be an orbital overlap between the two species. As the electron density decreases exponentially with distance from the nucleus, this means that the efficiency of DET decreases exponentially with the intermolecular distance R_{DA}. The rate constant of DET is expressed according to Equation 2.6

$$k_{DET} \propto Jexp(-2R_{DA}/L) \tag{2.6}$$

where J is the normalized spectral overlap, and L the effective orbital radius.[20] As a result, the Dexter mechanism works primarily at shorter distances (< 10 Å). In fluid solutions the DET happens through collisions between the species following diffusion and is mediated by high acceptor concentration. From the Stern-Volmer relationship of Equation 2.7 the efficiency of energy transfer as a result of diffusion can be obtained:

$$\frac{F_D}{F_{DA}} = \frac{\tau_D}{\tau_{DA}} = 1 + k_{TET}\tau_D[A] \tag{2.7}$$

F is the donor emission intensity, τ is the excited state lifetime of the donor, k_{TET} is the bimolecular quenching constant, and A is the acceptor concentration. Subscripts D and DA indicate when the donor is alone and when the acceptor is also present in the solution, respectively. Thus, by measuring the resulting quenching of the donor emission with respect to acceptor concentration, k_{TET} may be estimated. The resulting efficiency of the energy transfer, Φ_{TET}, can then be expressed by Equation 2.8

$$\Phi_{TET} = 1 - \frac{F_{DA}}{F_D} = 1 - \frac{1}{1 + k_{TET}\tau_D[A]} \tag{2.8}$$

In this thesis the *triplet-triplet* Dexter energy transfer is the one of greatest interest and will henceforth be referred to as TET.

2.2.2 Triplet-triplet annihilation

At the very core of photon UC lies the mechanism that is called *triplet-triplet annihilation* (TTA). The energy transfer mechanisms presented in Section 2.2.1, and especially TET, is of vital importance for TTA to function. The full process presented here is often referred to as *sensitized triplet-triplet annihilation upconversion* (sTTA-UC) and is presented in the Jablonski diagram of Figure 2.3. Since two photons are needed in order to produce one upconverted photon, it all begins with that two *sensitizer* (S) molecules (or particles) absorb one photon each and are excited to their first excited singlet states, denoted $^1S^*$ (Equation 2.9a). The excitation is followed by ISC to the sensitizer triplet excited state, $^3S^*$ (Equation 2.9b).

At this point, the two triplet excited sensitizers interact with two ground state *annihilator* molecules via TET, thus creating two triplet excited annihilators, $^3A^*$ (Equation 2.9c), while the sensitizers return to their respective singlet ground states, ^1S. The two triplet excited annihilators now interact to form one *singlet* excited state ($^1A^*$) annihilator and one singlet ground state (^1A) annihilator (Equation 2.9d). The excited annihilator then return to its ground state, emitting a photon of shorter wavelength than that of the two previously absorbed photons (Equation 2.9e). ν_{abs} indicates the frequency of photons initially absorbed while ν_{em} is the

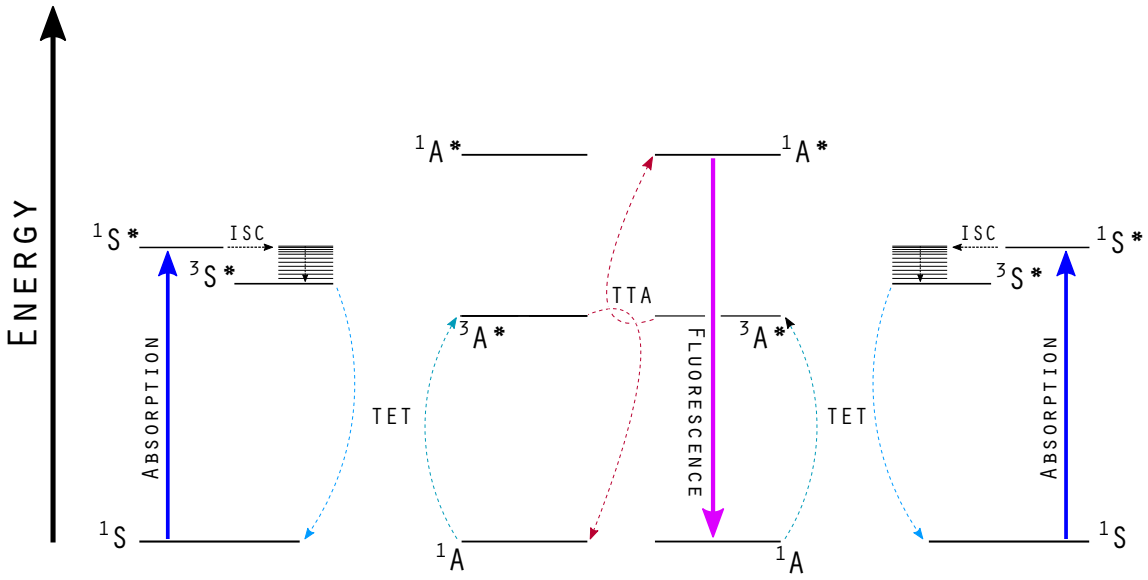


FIGURE 2.3: The ideal triplet-triplet annihilation mechanism. S and A denotes sensitizer and annihilator, respectively, while superscripts denote spin multiplicity. Photon absorption by the sensitizer is followed by intersystem crossing (ISC) to its triplet excited state. Subsequent triplet energy transfer (TET) populates the annihilator triplet excited states, which can then perform triplet-triplet annihilation as they meet. The singlet excited annihilator then emits one upconverted photon.

frequency of the upconverted, emitted photon.

$$\text{Absorption: } 2 \times [^1S + h\nu_{abs}] \rightarrow 2 \times [^1S^*] \tag{2.9a}$$
$$\text{Intersystem crossing: } 2 \times [^1S^*] \rightarrow 2 \times [^3S^*] \tag{2.9b}$$
$$\text{Triplet energy transfer: } 2 \times [^3S^* + {}^1A] \rightarrow 2 \times [^1S + {}^3A^*] \tag{2.9c}$$
$$\text{Triplet-triplet annihilation: } 2 \times [^3A^*] \rightarrow {}^1A^* + {}^1A \tag{2.9d}$$
$$\text{Emission: } {}^1A^* \rightarrow {}^1A + h\nu_{em} \tag{2.9e}$$

However, the process isn't as straight-forward as it might appear. For instance, the final annihilation step can produce several different outcomes. Because of the spin multiplicity, M_s, of the triplet state, $3 \times 3 = 9$ different combinations can be created as two triplet excited molecules undergo TTA. This will results in either a singlet, a triplet, or a quintet state. Spin statistics dictate the probabilities for the formation of these and is directly related to the value of M_s for the respective states. The probabilities, f, of formation are thus 1/9 for singlets, 3/9 for triplets, and 5/9 for quintets. Equations 2.10a-2.10c show the pathways for the formation of the different states.

$$^3A^* + {}^3A^* \rightleftharpoons {}^1(AA)^* \rightarrow {}^1A^* + {}^1A \tag{2.10a}$$
$$^3A^* + {}^3A^* \rightleftharpoons {}^3(AA)^* \rightarrow {}^3A^{**} + {}^1A \rightarrow {}^3A^* + {}^1A \tag{2.10b}$$
$$^3A^* + {}^3A^* \rightleftharpoons {}^5(AA)^* \rightarrow {}^5A^* + {}^1A \tag{2.10c}$$

The maximum singlet state yield of TTA is statistically thus 11,1%, but this limit can be exceeded[21] because of the quintet states generally being energetically inaccessible. The fact that triplets are regenerated in the pathway of Equation 2.10b means that the collision of four triplet pairs (three collisions following the pathway of Equation 2.10b, one collision following the pathway of Equation 2.10a) destroys five triplet states in total. Out of these, two states are involved in the formation of one singlet state. Disregarding the pathway of Equation 2.10c, one thus instead gets a probability of $f = 2/5$ for singlet formation.[22] Furthermore, if the second excited triplet state T_2 (see Figure 2.1) also is too high in energy the triplet formation pathway in Equation 2.10b is also inaccessible, leading to a theoretical singlet formation yield of unity.[22]

2.2.3 sTTA-UC efficiency

Of interest in the scope of this thesis is of course the efficiency that can be achieved from a successful sTTA-UC process. To measure this the *upconversion quantum yield*, Φ_{UC}, is generally used. It measures the ratio between emitted upconverted photons, and absorbed photons. Φ_{UC} is often defined as in Equation 2.11

$$\Phi_{UC} = f \times \Phi_{ISC} \times \Phi_{TET} \times \Phi_{TTA} \times \Phi_f \tag{2.11}$$

where f is the probability factor related to the spin statistics, Φ_{ISC} is the efficiency of sensitizer intersystem crossing, Φ_{TET} the TET efficiency, Φ_{TTA} the TTA QY, and Φ_f the fluorescence QY of the annihilator. As the sTTA-UC requires two low-energy photons for each upconverted high-energy photon, the Φ_{TTA} can take on a maximum value of 50%. This is also the maximum value for Φ_{UC} since the remaining terms all may approach unity.

To maximize Φ_{TET} the system needs a high annihilator concentration, $[A]$. The TET from sensitizer to annihilator (which strongly relates to k_{TET} from Subsection 2.2.1.2) competes with other decay processes of the $^3S^*$ state. Since TET is diffusion controlled, a high annihilator concentration will help enhance the efficiency of TET. Similar arguments for high annihilator concentrations can be presented for maximizing Φ_{TTA}; if $[^3A^*]$ is high the TTA efficiency will increase.

This is also related to the intensity of the excitation light that is used for UC. For a diffusion controlled system there are two different regimes that behave a bit differently. At low excitation energies, $[^3A^*]$ will be quite low and thus the TTA process will compete with other decay mechanisms. This results in a system where the UC emission depends quadratically on excitation intensity at low intensities, and where Φ_{UC} depends linearly on intensity. In the second regime, where excitation intensities are higher, $[^3A^*]$ will also be higher and TTA will be the dominating decay mechanism, working as efficiently as possible. This leads to a linear dependence on excitation at high intensities, or that Φ_{UC} is independent on intensity. At the crossing between the quadratic and linear intensity dependence we find the *threshold intensity*, I_{th}. For an optimal sTTA-UC system it is given by Equation 2.12:[23,24]

$$I_{th} = \frac{k_{TA}^2}{2k_{TTA}\alpha[^1S]} \tag{2.12}$$

where k_{TA} is the triplet decay of the annihilator and α the molar extinction coefficient of the sensitizer. Since the average sunlight intensity is quite low (circa 10 mW/cm^2) one strives for a low I_{th}. It is therefore of great importance to try and create systems with high k_{TTA}.

2.3 Sensitizers and annihilators for upconversion

There are many different aspects to consider when it comes to achieving successful UC, such as choosing suitable sensitizer and annihilator compounds. From Figure 2.3 it is obvious that a number of energy levels inherent for each compound must be considered, and of special interest are the sensitizer and annihilator singlet and triplet excited state energies. For the TTA process to work properly the following points must be fulfilled by the sensitizer:

- It should effectively absorb light of desired wavelength
- The ISC from $^1S^*$ to $^3S^*$ must be efficient
- Low energy splitting between $^1S^*$ and $^3S^*$
- $^3S^*$ must be quite longlived (>10 μs) to permit TET to take place
- Small spectral overlap with annihilator emission to avoid FRET from annihilator to sensitizer following TTA

Similar requirements can be put on the annihilator compounds. The annihilator of choice should have:

- a high fluorescence QY
- a triplet excited state energy slightly below that of the sensitizer (E[$^3A^*$] < E[$^3S^*$])
- a singlet excited state energy that do not surpass that of two times its triplet excited state energy (E[$^1A^*$] < 2 × E[$^3A^*$])
- energetically inaccessible quintet states ($^5A^*$) and second excited triplet states ($^3A^{**}$), if possible

As it turns out it is not always easy to fulfill all criteria. For vis-to-UV UC there will be several limiting factors that may be attributed to one or several of the aforementioned prerequisites.

2.3.1 CdS/ZnS core-shell nanoparticles

Semiconductor core-shell nanoparticles (NPs) have previously been used for UC into the near infrared and visible spectrum[25,26,27] and as of last year also for vis-to-UV UC.[15] The strength of semiconductor NPs mainly lie within the possibilities in tuning their properties, something that originates from the innate energy dispersion of nanosized materials. NPs have at least one dimension on the nanometer scale, meaning that their size are in the same range as molecules. It is therefore not surprising that the intrinsic energies of semiconductor NPs are a mixture between the energies of a bulk semiconductor and that of molecules. In detail this means that there is a band gap, very similar to that of a bulk semiconductor, but like with molecules there are discrete energy levels in NPs.[28] Compared to molecules, this energy level splitting is however much smaller in NPs but since particles can be of different size this splitting may also be tuned.[29] An example of this is that the larger the NP is, the smaller its corresponding band gap will be.[30]

Using semiconductor NPs as a sensitizer for vis-to-UV UC holds great promise as this kind of sensitizer currently holds the vis-to-UV QY record.[15] This study will utilize the same sensitizer as the record report, a core-shell type NP with a cadmium sulfide (CdS) core and a zinc sulfide (ZnS) shell structure.[15,31] Bulk CdS has a band gap of 2.5 eV[32] and also exhibits a high molar extinction coefficient, ε,[33] making CdS an excellent absorber of blue light. This absorption is however also strong in the UV region, leading to a severe spectral overlap between sensitizer absorption and annihilator emission. This will inhibit detected UC due to quenching mainly by reabsorption of upconverted light by the NPs. The band gap width of the NPs can however be tuned, meaning that one can match it with the desired wavelength of the light one wants to absorb. As cadmium is a quite heavy metal (M = 112,41 g/mol) the CdS NPs will also exhibit a large spin-orbit coupling.[34] This will increase the rate of ISC, a process that must be effective in order to achieve a high triplet state yield in the sensitizer.

Even though semiconductor NPs holds great promise for sensitization, there are certainly difficulties that need to be addressed. With the small size of the particles comes a high surface to volume ratio. Surface sites are special in the sense that the electrons and orbitals of these are not shared with any neighbouring atoms. A high number of non-interacting orbitals, generally referred to as ”dangling bonds”, may lead to low energy trap states within the NP.[15] These are detrimental to NP emission and should thus be avoided, and may be passivated by different ligands, such as carboxylic acids.[25,26] This will also enhance the efficiency of TET from sensitizer to mediator.[15,26] Another way to reduce the amount of trap states is by the growth of a shell, and the addition of several layers will lead to increased NP emission.[15,31] However, the shells will also provide a tunneling barrier,[35] decreasing the TET efficiency and thus leading to decreased UC. It has however been determined (at least in one study) that four ZnS monolayers give the highest value of Φ_{UC} when sensitizing with CdS/ZnS core-shell NPs.[15]

Another issue with semiconductor NPs are their short triplet lifetimes. They typically have a triplet lifetime on the order of a few nanoseconds,[15,25] which is orders of magnitudes shorter than the triplet lifetime needed for efficient TET to the annihilator. This issue can be overcome by the addition of a transmitter ligand,

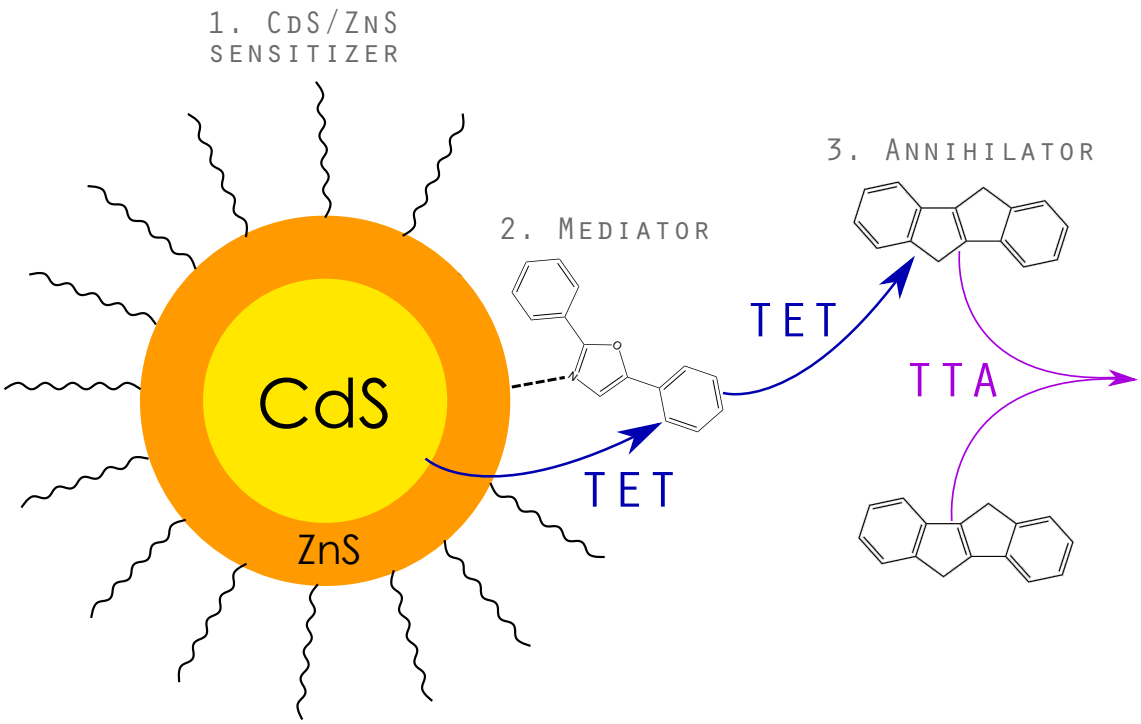


FIGURE 2.4: Energy transfer schematic for the usage of a mediator. The mediator, here represented by 2,5-diphenyloxazole (PPO), binds to a zinc site of the CdS/ZnS NP via a nitrogen atom. This bond enables TET from sensitizer to mediator. Subsequent TET from mediator to an annihilator in solution is followed by TTA between two annihilator molecules. For a more detailed description of the energetic relationships, see Figure 2.3.

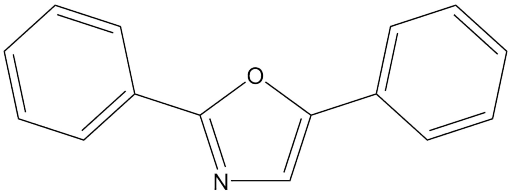
referred to as the *mediator*, which binds to the NP surface through an anchoring group, and by doing so replaces one of the oleic acid ligands already present at the surface.[25,26] In Figure 2.4 this path for energy transfer is illustrated. TET from the NP to the mediator leads to a prolonged triplet lifetime and enables further TET to the annihilator molecules which are free in solution. For this to happen the triplet energy of the mediator must of course lie in between the respective energies of the sensitizer triplet excited state, $^3S^*$, and annihilator triplet excited state, $^3A^*$ (see Figure 2.3).

2.3.2 Annihilator candidates

The number of suitable sensitizer-annihilator pairs for vis-to-UV has so far been quite limited, and there is a need to expand the knowledge around why that is the case. Not only has it been almost impossible to find pairs which fulfill all the criteria mentioned previously (in the case of using CdS/ZnS NPs as sensitizer, the spectral overlap will certainly be an issue), but even if the criteria are fulfilled this do not necessarily lead to efficient UC.[24]

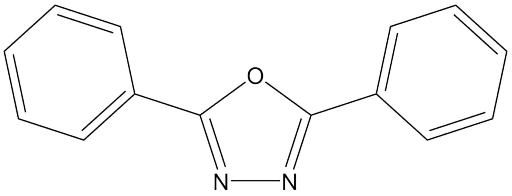
In this study an endeavour to try and find new possible annihilators for vis-to-UV UC is undertaken. The annihilator candidates of interest are presented in Figure 2.5. All selected compounds have a high fluorescence QY,[18,36,37,38,39,40] and have a first triplet excited energy which lie below that of previously synthesized

CdS/ZnS sensitizers.[15] The presented values for their respective energies should not be considered absolute, as these have been calculated using Density Functional Theory. These values do however give some important indications on their eligibility as annihilators. The calculations do e.g. tell us that their second excited triplet state, T_2, lie between T_1 and S_1 in energy, resulting in an expected f value of no higher than 2/5 (the importance of the f value is discussed in Section 2.2.2).



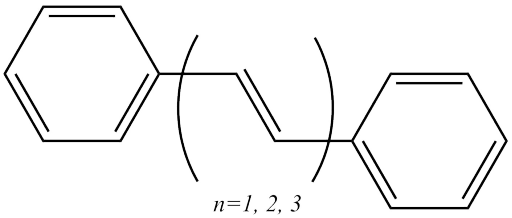
(A) 2,5-diphenyloxazole (PPO)

$E(T_1)$	$E(T_2)$	$E(S_1)$	$2 \times E(T_1) - E(S_1)$
2.521 eV	3.35 eV	3.880 eV	1.16 eV



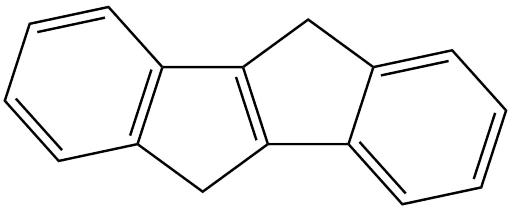
(B) 2,5-diphenyl-1,3,4-oxadiazole (PPD)

$E(T_1)$	$E(T_2)$	$E(S_1)$	$2 \times E(T_1) - E(S_1)$
2.844 eV	3.34 eV	4.165 eV	1.52 eV



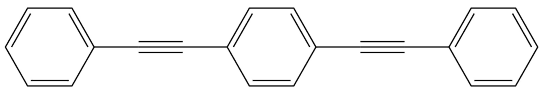
(C) trans-stilbene (TS) and derivatives

	$E(T_1)$	$E(T_2)$	$E(S_1)$	$2 \times E(T_1) - E(S_1)$
n=1	2.296 eV	3.64 eV	4.004 eV	0.59 eV
n=2	1.832 eV	3.23 eV	3.577 eV	0.087 eV
n=3	1.506 eV	2.82 eV	3.234 eV	-0.22 eV



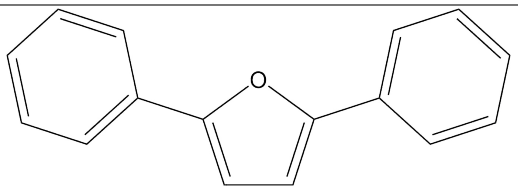
(D) 5,10-dihydroindeno[2,1-a]indene (I2)

$E(T_1)$	$E(T_2)$	$E(S_1)$	$2 \times E(T_1) - E(S_1)$
2.389 eV	3.64 eV	3.897 eV	0.88 eV



(E) 1,4-bis(phenylethynyl)benzene (BPB)

$E(T_1)$	$E(T_2)$	$E(S_1)$	$2 \times E(T_1) - E(S_1)$
2.252 eV	3.00 eV	3.440 eV	1.06 eV



(F) 2,5-diphenylfuran (DPF)

$E(T_1)$	$E(T_2)$	$E(S_1)$	$2 \times E(T_1) - E(S_1)$
2.351 eV	3.34 eV	3.754 eV	0.95 eV

FIGURE 2.5: The eight different annihilator candidates. The energy values have been calculated using Density Functional Theory and give indications on each compounds potential for UC. The value of greatest importance is that in the right-hand side column, which must be positive in order for TTA to happen.

Even more important, the calculated values give an indication on the driving force of TTA, which solely depends on the energy requirement $E[^1A^*] < 2 \times E[^3A^*]$. A positive value in the right-hand column for each annihilator indicates that this equation holds true for that particular compound.

Out of the proposed annihilators, 2,5-diphenyloxazole (PPO) is the only one

that has previously been tested for UC, and successfully so.[15,16,41] A very similar compound, 2,5-diphenyl-1,3,4-oxadiazole (PPD), will here be investigated alongside PPO. PPD has a slightly higher S_1 energy, meaning that successful UC using PPD would increase the resulting anti-Stokes shift. These two compounds are of special interest as this study aims also to determine which of these is most suitable in the role of mediator. PPO has been utilized before,[15] but the slightly higher T_1 energy of PPD might decrease energy losses during ISC from the CdS/ZnS. This energy could however be too high in relation to the sensitizer triplet energy if the sensitizer particle size is suboptimal.

The three derivatives related to trans-stilbene (Figure 2.5c) has, to the best of my knowledge, not been utilized as annihilators before. The addition of more double bonds in the bridge between the two phenyl rings seem to destabilize the singlet and triplet energies, and also - in the case of n=3 - the triplet energy seem to be too low in relation to the singlet energy. For the trans-stilbene (TS, n=1) it is well known that it easily isomerizes into its *cis*-isomer in low-viscosity solvents, something that effectively inhibits the fluorescence QY.[18,42] This distortion of the structure does however not seem to appear for 1,4-diphenyl-1,3-butadiene (DPB, n=2).[43] For 1,4-diphenyl-1,3,5-hexatriene (DPH, n=3) the transition to other conformations has been found in polar solvents, which has reduced fluorescence, but has not been observed in non-polar solvents, such as hexane.[44] Similar conformational changes has been observed for 1,4-bis(phenylethynyl)benzene (BPB), as it may rotate around its triple bonds. The cylindrical symmetry of these bonds means that the conjugated system remains intact, but also that the the resulting emission is shifted.[45]

To overcome potential issues with isomerization that arise for these stilbenes, the locked stilbene 5,10-dihydroindeno[2,1-a]indene (I2), will be investigated as an alternative. Similar to trans-stilbene, it has a high fluorescence QY near unity[39] but is locked in its *trans*-isomer.[46] Regarding the calculated values, I2 seems to be a promising compound for the role of annihilator, but hasn't been tried previously. Finally, 2,5-diphenylfuran (DPF) will be investigated. Its similarities to PPO and PPD are very pronounced, but the lack of nitrogen atoms give rise to slightly lower energies, thus decreasing the potential anti-Stokes shift.

3
Methods

This section aims to present the different methods and experimental techniques that have been utilized during the course of this study. The experimental work spans over two distinct, and quite different, branches: spectroscopy experiments and NP synthesis.

3.1 Spectroscopic methods

Any physical chemist will sooner or later encounter different kinds of spectroscopy. It provides a powerful tool that can be applied to a large variety of molecules. In this study it has been one of the main tools for characterizing the participating compounds. All spectroscopic measurements performed in this study has been carried out in hexane, C_6H_{14}, a non-polar, low-viscosity solvent, and the samples were placed in a 4mm quartz cuvette.

3.1.1 Steady-state absorption spectroscopy

To determine the average absorbance of a compound one can employ steady-state absorption spectroscopy. The setup used for this technique is presented in Figure 3.1. Light passes through a monochromator which selects which wavelength is transmitted. As the selected light reaches the beam splitter, a small fraction is reflected to a reference detector, and the larger part of the light passes through to the sample. The sample detector then measures how much of the incident intensity, $I_0(\lambda)$, that passes through the sample.

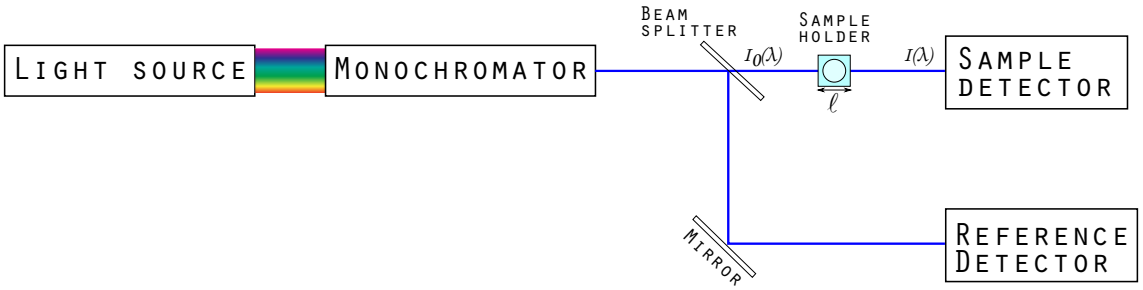


Figure 3.1: The experimental setup for absorption measurements. The monochromator selects one wavelength at the time and the sample detector measures the intensity of non-absorbed light. Sweeping over a range of wavelengths in the monochromator creates an absorption spectrum of the sample.

The absorbance relates to the incident and transmitted intensities through

$$Abs(\lambda) = -log\ \frac{I(\lambda)}{I_0(\lambda)} \tag{3.1}$$

which in turn relates to concentration through the *Lambert-Beer law*:

$$Abs(\lambda) = \varepsilon(\lambda)cl \tag{3.2}$$

where ε is the molar extinction coefficient (M^{-1} cm^{-1}), c is sample concentration (M), and l is the path length the light travels through the sample (cm). Absorbance is thus unit free, and a compound with a high ε will absorb more strongly. Since ε is wavelength dependent, the absorption spectrum of a compound is obtained by scanning over a range of wavelengths.

3.1.2 Emission spectroscopy

Absorption measurements are commonly performed alongside emission measurements. A similar setup is used for steady-state emission spectroscopy, but with a few modifications, see Figure 3.3. A monochromator selects the wavelength you want to use to excite your sample. As excited molecules (or particles) relax to their ground state, the emitted fluorescence is detected. However, in order to account for any fluctuations in excitation light intensity, a small portion of the incident light is directed to a reference detector. A second monochromator is used after the sample to select what wavelength of emitted light that will be detected. Typically one uses a single excitation wavelength, and sweeps over a range of wavelengths in the emission monochromator.

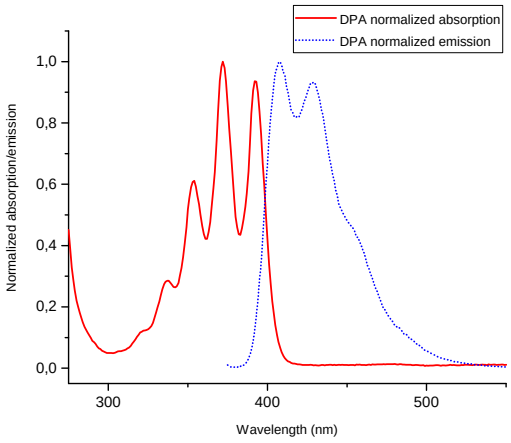


FIGURE 3.2: Normalized absorption and emission spectra for the common fluorophore 9,10-diphenylanthracene (DPA).

The absorption and emission spectra of fluorophores are often presented alongside each other, and an example is given in Figure 3.2. This is the spectra of 9,10-diphenylanthracene (DPA), a molecule that is well known for its high fluorescence QY and has been widely used as a fluorescence reference compound.[47,48] It just happens so that it is also one of the most used annihilators for UC, producing blue upconverted light through TTA.[12,49,50,51] In this study DPA will be used as a fluorescence QY reference compound. By measuring the absorption of a compound of interest and a reference compound, and their respective emission at the same excitation wavelength, the fluorescence QY of the sample compound ban be determined by Equation 3.3:[48]

$$\Phi_{f,s} = \Phi_{f,r}\frac{F_s}{F_r}\frac{A_r}{A_s}\frac{n_s^2}{n_r^2} \tag{3.3}$$

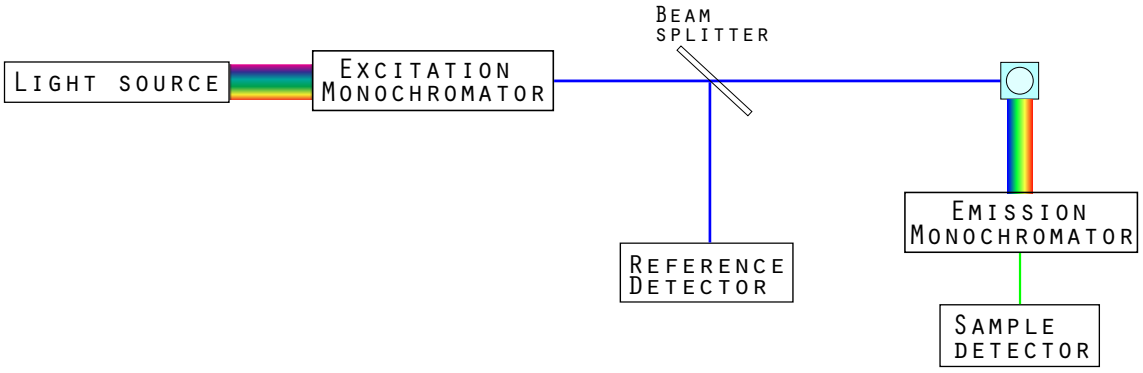


Figure 3.3: The experimental setup for emission measurements. The difference from an absorption measurement setup is that the excitation monochromator typically is fixed at one specified wavelength, and that the sample detector measures the emission from the sample. A second monochromator selects one wavelength at the time that is allowed to pass, and by sweeping over a range of wavelengths an emission spectrum may be obtained.

Here, Φ is the fluorescence QY, F is the integrated emission, A is the measured absorption at the excitation wavelength, and n is the refractive index of the solvent used. Subscripts r and s denotes reference and sample, respectively. The same expression may also be used to calculate UC QY.

3.1.2.1 Time-resolved emission spectroscopy

Steady-state emission can be used to determine e.g. fluorescence QY, but strongly related to that is the fluorescence lifetime, often denoted τ_f. To measure this a very similar setup to that of the steady-state case is used. The main differences are the type of excitation light used, and how the emission is detected. Time-resolved measurements are often performed using a technique called *time correlated single photon counting*, TCSPC. Instead of non-coherent light, a pulsed laser is used for excitation of the sample. A timer measures the time from excitation to when the first emitted photon reaches the detector. The time is recorded and the process repeated. The average lifetime τ_f can then be determined from the measurements.

This kind of measurement will result in a histogram with time between excitation and detected emission on the x-axis, and number of counts on the y-axis. The time scale is divided into discrete channels, and for every measurement one of these channels will be filled with a photon count. Depending on how resolved one wants the measurement to be, the number of channels may be altered. Since the excitation pulse is not a perfect Dirac pulse, and one often are measuring on very short time scales, an *instrument response function* (IRF) must be measured with a scattering sample and taken into account for.

3.1.3 Upconversion measurements

Means of measuring UC do not differ that much from ordinary emission techniques. Typically a laser is used for excitation of the sample, and the output emission is measured perpendicularly to that of the incident laser light. The light intensity may

then be varied to form data plots which may indicate where the intensity threshold (I_{th}, see Section 2.2.3) lie.

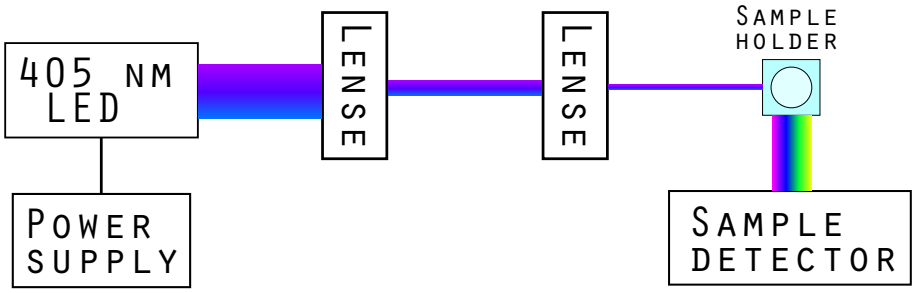


FIGURE 3.4: The experimental setup for UC measurements. Two lenses are employed to focus as much of the diverging light from the LED as possible. The power supply drives the lamp, and can be used to alter the light intensity from the LED.

This study unfortunately makes use of a somewhat suboptimal setup, see Figure 3.4. Due to the absence of a suitable laser for excitation at the facilities, a 405 nm light-emitting diode (LED) lamp has been utilized instead. This non-coherent light source emits a strongly diverging light, meaning that only a tiny fraction of the outgoing intensity would reach the sample if no modification was done. Two converging lenses has for this reason been positioned between the LED and sample in order to maximize intensity at the sample. The LED is driven by an external power supply, and the light intensity may be varied by changing the supplied current. Due to this particular setup, the detector will not only receive the emitted light from the sample, but also traces of light from the LED lamp. In a setup where a laser is employed, a notch filter would have been placed between the sample and the detector to cut away any light from the excitation source, thus ensuring that only emitted light from the sample reaches the detector.

3.2 CdS/ZnS core-shell NP synthesis

The CdS/ZnS core-shell NP synthesis consists of two separate steps: core synthesis and shell growth, and is visualized in Figure 3.5. The approach used for CdS core synthesis is often referred to as the *hot injection method*,[52] as the sulfur precursor is injected at very high temperature (∼260 °C). The full and detailed recipe is presented in the following paragraph. All solvents were degassed prior to use, and five batches of CdS/ZnS particles were synthesized in total.

3.2.1 CdS core synthesis

257 mg cadmium oxide (CdO) was mixed with 6 mL oleic acid and 15.8 mL 1-octadecene (ODE) in a 50 mL three-necked bottle. The middle neck was connected to a condenser and the two remaining necks were sealed with septums. The flask was placed on a temperature controlled heat block, and the mixture was degassed under vacuum for 1 hour at 110 °C. This was followed by heating of the mixture to 260 °C under nitrogen, which resulted in a clear and colorless reaction mixture. The

sulfur precursor was prepared by adding 32 mg of sulfur powder to 3 mL ODE in a glovebox (which is a sealed container with a low oxygen, low water atmosphere), followed by sonication of the solution. The precursor was injected at 240 °C and then stirred until the mixture had attained a rich, yellow color (this took about one minute). The mixture was then cooled using compressed air. After cooling, a small sample of the mixture was mixed with hexane in a 10mm quartz cuvette for characterization through absorption spectroscopy.

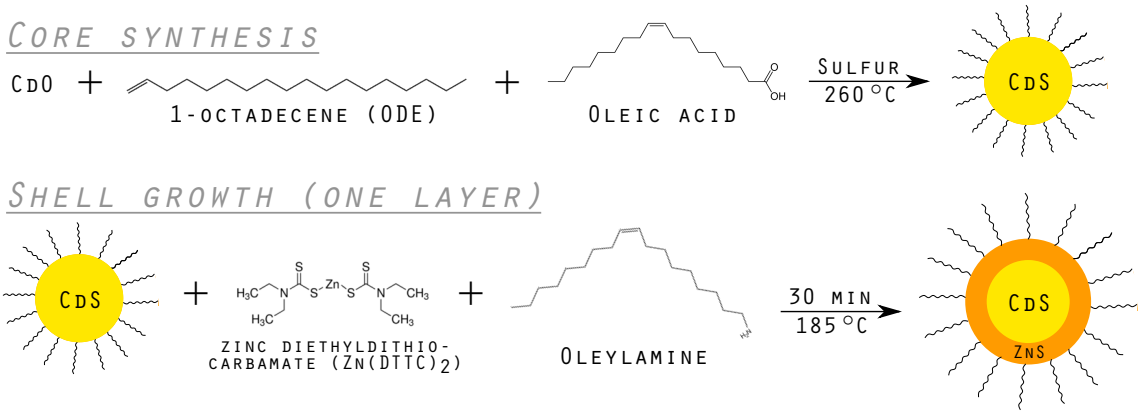


FIGURE 3.5: Synthesis scheme for the production of CdS/ZnS core-shell NPs. The CdS cores are synthesized by addition of sulfur powder at high temperature. Subsequent shell growth is done by addition of the zinc precursor $Zn(DTTC)_2$ and stirring at ∼185 °C. The shell growth procedure was repeated four times. The wiggly lines on the surface are ligands of oleic acid.

The CdS cores, which are capped with oleic acid ligands, were then transferred to a degassed 27 mL vial, which was in turn transferred into a glovebox. A purification scheme where the CdS cores were extracted by methanol, hexane, and butylamine (1:0.7:0.04 volume ratio) followed. The cores had a tendency to create a gel-like solution if stored too long in ODE, and the addition of 50 μL butylamine was used to liquefy the solution. The addition and subsequent mixing of methanol and hexane resulted in a two-phase mixture. The upper methanol phase was removed with a pipette and methanol was added again for further purification. After subsequent removal of the methanol, the mixture was transferred to a 50 mL centrifuge vial, and an excess of acetone (∼40 mL) was added. The mixture was then centrifuged, resulting in a yellow precipitate at the bottom of the centrifuge vial. The precipitated CdS cores were then redispersed in hexane, and another round of acetone addition and centrifugation followed. Finally, the precipitate was redispersed in hexane for long-term storage.

3.2.2 ZnS shell growth

The absorption spectrum obtained from the CdS core sample was not only used to characterize the particles but also to measure the amount of particles in the sample.

By taking 10 μL of CdS core solution and measuring its absorbance in hexane, the concentration could be determined using the the Lambert-Beer law (Equation 3.2). The molar extinction coefficient, ε, and expected diameter of the CdS cores could also be determined from the spectrum.[33] Knowing the concentration of particles in the cuvette, the total number of synthesized particles could be calculated.

For the ZnS shell growth the amount of the zinc precursor, zinc diethyldithiocarbamate ($Zn(DTTC)_2$), needed for each monolayer (ML) was calculated.[31] The full calculation can be found in Appendix A.1. Once calculated, the required total amount of $Zn(DTTC_2)$ (365 mg) was mixed with 10 mL oleylamine to create a 0.1 M solution, which was sonicated for 200 seconds for increased solubility. The CdS cores were dissolved in 12.23 mL ODE, degassed, and put to stirring in a three-necked bottle. 0.723 mL of 0.1 M $Zn(DTTC_2)$ was then added, and the mixture was heated to 185 ℃. It was left to react for 20 minutes before the mixture was cooled to 50 ℃. The procedure was then repeated for the next three MLs. For each ML the mixture was heated and stirred for circa 30 minutes. A small sample of the mixture was extracted and absorption and emission measurements were performed in hexane for characterization during each step.

Following the shell growth, the CdS/ZnS NPs were purified inside a glovebox. The NPs in ODE were transferred to a centrifuge vial, an excess of methanol was added, and the mixture was shaken vigorously. The two phases were allowed to separate and the upper, low viscosity methanol phase was removed by pipette. This was repeated two more times. An excess of acetone was then added to the vial and the mixture was centrifuged for 15 minutes. The supernatant was removed and the yellow precipitate that had formed was dispersed in hexane. The acetone purification step was repeated two more times before the NPs were redispersed in hexane for long-term storage inside the glovebox.

3.2.3 Mediator/ligand exchange and UC measurements

To evaluate how well the respective mediator molecule binds to the ZnS shell of the NPs, both absorption and emission spectroscopy have been utilized. The different samples have been prepared so that the ratio between CdS/ZnS NP concentration and PPO concentration was either 1:10 or 1:1000. This was done in order to investigate if PPO would bind stronger onto the NPs if this ratio was altered. The NP concentration c were for all samples in the range of 10 to 100 nM.

The preparation of the samples were made by calculating what amounts of NPs and mediator respectively that would be needed to achieve the desired ratio between the two compounds. These were then mixed and stirred in a small vial, located in a glovebox. Different samples were stirred for different amounts of time, ranging from 5 minutes to 24 hours, in order to determine if time was a factor. Following the stirring, each sample was precipitated in acetone and centrifuged to remove excess mediators that was left free in solution.

The samples for UC measurements were prepared by dissolving the different annihilators in hexane, thus creating solutions with [A] = 5.7×10^{-2} M. These stock solutions could then be used to create the UC systems, with concentrations [A] = 5.7×10^{-3} M and [CdS/ZnS] = 2.85×10^{-7} M. These samples were not cleaned or

stirred following the mixing of compounds, and measurements could be performed instantly after sample preparation.

4
Results and Discussion

The following section aims to present the key findings of this study. NP synthesis is analyzed both in terms of experimental setup but also by means of absorption and emission spectroscopy. Ligand exchange with the mediators and annihilator characterization has mainly been investigated through absorption and emission spectroscopy.

4.1 Synthesis of CdS/ZnS core-shell NPs

As has been previously mentioned, a total number of five batches were synthesized during the course of this study. The main reason for this was the desire to synthesize a sensitizer of higher quality than that of previous batches.

4.1.1 Initial characterization of CdS/ZnS NPs

As it turns out, the very first batch of CdS/ZnS NPs that was made was the one that exhibited the best characteristics. Table 4.1 shows the photophysical characteristics of the NPs for each of the synthesized batches. Only the first batch went unscathed through all synthesis steps. Batch no. 2 and 4 both failed during the initial CdS core synthesis. Batch no. 3 failed during the ZnS shell growth, and the last batch was discarded as the final purification step went awry. This batch did however show less emission than batch no. 1 and would for this reason not have been used anyway.

TABLE 4.1: Absorption and emission characteristics of the five synthesis efforts. Two batches failed completely and did not return any detectable particles at all. Batch 3 went awry during the ZnS shell growth, and the very last batch was discarded as a result of issues in the final purification step.

Batch no.	Abs_{max}(CdS) (nm)	Abs_{max}(CdS/ZnS) (nm)	Em_{max} (nm)
1	408	430	445
2	-	-	-
3	403	-	-
4	-	-	-
5	395	442	463

The very first batch resulted in functioning CdS/ZnS NPs with an absorption maxima at 430 nm, and an image of the NPs obtained through *transmission electron microscopy*, TEM, is presented in Figure 4.1. From the absorption maxima it

was expected that the diameter of the NPs would be roughly 4.5 nm.[33] The size distribution is quite uniform but a bit larger than expected, and also the shape of the NPs is not entirely spherical.

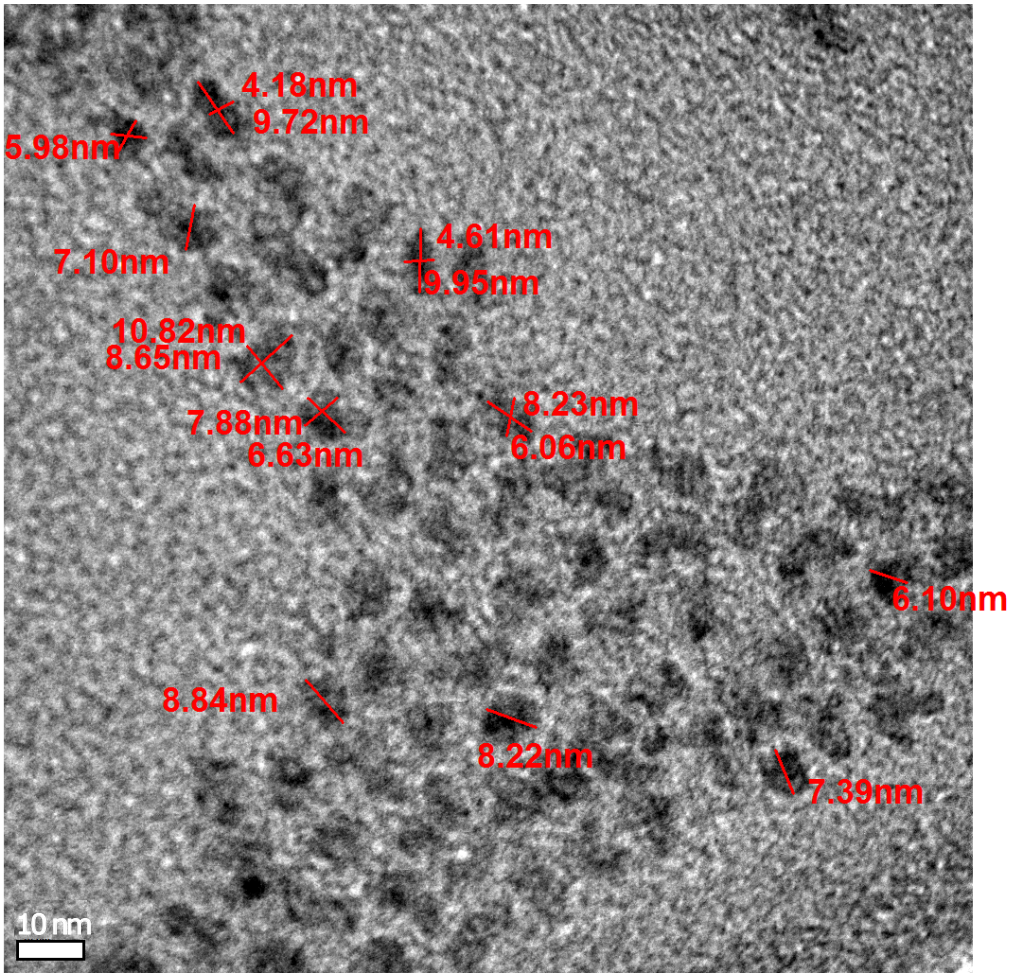


FIGURE 4.1: Image of the CdS/ZnS NPs obtained through TEM. The NP size is generally a bit larger than the expected 4.5 nm in diameter, and the shapes are slightly non-uniform.

Questions about the NP quality did arise, mainly as a result of lower than expected photoluminescence QY, Φ_{PL}, of the NPs. Previous studies where CdS/ZnS NPs have been synthesized have shown Φ_{PL} as high as 50%,[31] while the NPs used by Gray *et al.* reached $\Phi_{PL} = 26\%$.[15] Batch no. 1 in this study yielded $\Phi_{PL} = 7.3 \pm 0.3\%$, which is almost one magnitude lower than what has previously been achieved.

Some important characteristics of CdS/ZnS NPs are shown in Figure 4.2. The data presented here are for batch no. 5. The first thing to observe is a severe red-shift of the absorption (solid lines) local maxima, as it is shifted from 395 nm to 442 nm as the first ML of ZnS is added. This was expected, and is in fact a sign of successful shell growth without the formation of alloys.[31] This shift to lower energies is due to the difference between the energy levels of the NPs are narrowed as particle size is increased, and also due to possible deterioration of the size distribution.[53] The second thing to pay attention to is the destruction of emissive *trap states*, which can be seen for 0ML to 2ML in the 450 to 700 nm range. These are located at the surface

of the NPs and are a result of sulfur vacancies in the CdS core.[54] As three or more ZnS MLs are added it is evident that the emission from the trap states disappears, and along with that the NP emission peak (located at ∼463 nm in Figure 4.2) is greatly enhanced.

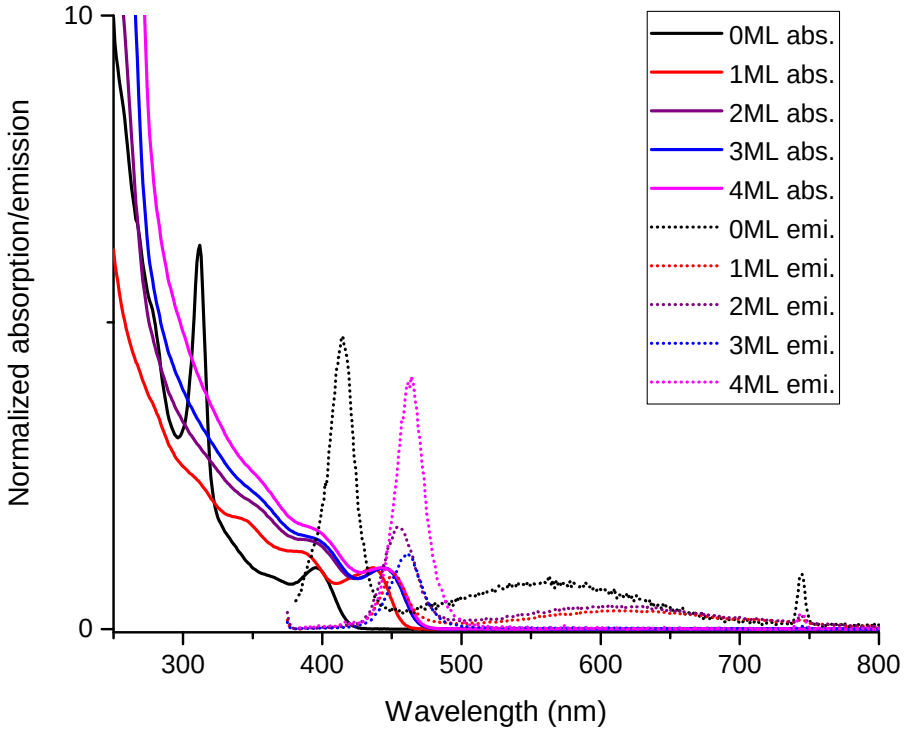


FIGURE 4.2: Absorption and emission of the batch no. 5 NPs during the different steps of shell growth. An immediate red-shift (from 395 to 442 nm for the absorption) is observed following the growth of the first ML. Growth of additional MLs effectively eliminates the emissive trap states that are seen in the range of 450 to 700 nm for 0ML to 2ML. Initially the NP emission is quenched as ZnS MLs are added, but as the 4th ZnS ML is added a severe increase of the emission is evident.

Time-resolved emission spectroscopy was also carried out on the NPs and the result is presented in Figure 4.3. The blue solid line represents the emission decay, and the black solid line is a best fit to these values. The red line is the IRF. In order to achieve sufficient fitting, three exponential terms were needed, which is a typical characteristic of NP photoluminescence decay.[15]

The intensity weighted average lifetime, $\bar{\tau}$, can be calculated using the values of the three exponentials provided from the best fit. Using Equation 4.1

$$\bar{\tau} = \frac{\sum_i A_i \tau_i^2}{\sum_i A_i \tau_i} \tag{4.1}$$

where A_i is the amplitude of the i:th exponential and τ_i is the lifetime of that component, an average lifetime $\bar{\tau} = 13.6$ ns was obtained for the CdS/ZnS NPs. This result is in the same range as previously reported lifetime values.[15] As suspected, the lifetime of the NPs is order of magnitudes shorter than what is needed to achieve efficient TET to the annihilators.

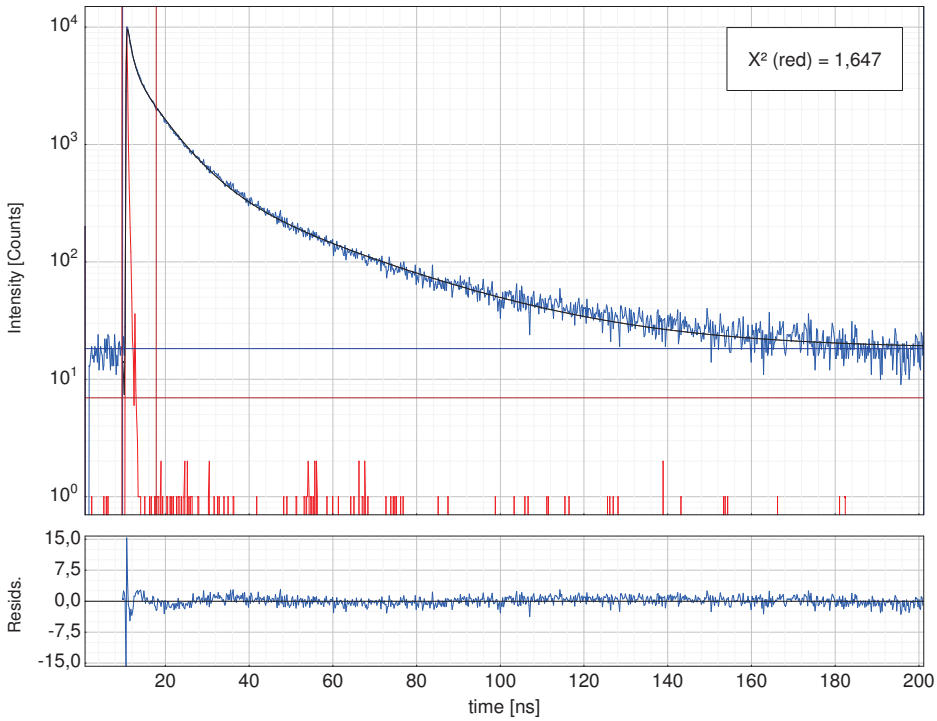


FIGURE 4.3: Time-resolved emission spectroscopy measurement on CdS/ZnS NPs. The black solid line is a best fit using three exponential terms. The measurement was done using 377 nm excitation light.

4.1.2 Synthesis considerations and optimization

From the previous section it is evident that synthesis of CdS/ZnS core-shell NPs is no walk in the park. The recipe that has been used during this study, based on efforts by Chen *et al.*,[31] Li *et al.*,[52] and Gray *et al.*,[15] is rather easy to follow and understand, as specific temperatures and chemical amounts are clearly printed.

The synthesis of the first three batches were carried out using the same exact experimental setup. Batch no. 2 failed due to contamination from a vacuum grease that is used to provide a seal between the reaction flask and the condenser pipe. This grease started dripping into the mixture, effectively destroying the reaction. This was adjusted before the next batch, which worked well during CdS core synthesis. Unfortunately, the human variable came into play during ZnS shell growth as insufficient attention to detail resulted in the wrong solvent being used for the zinc precursor.

After these rather trivial shortcomings had been fixed, the problems mainly arose from insufficient control of temperature and chemical amounts. Perhaps the biggest issue was controlling the temperature of the mixture. As mentioned in Section 3.2.1 a heat block was used for heating the reaction mixture, and a thermometer monitored the temperature of said heat blocks. Prior to the synthesis of batch no. 4 a new kind of heat block was introduced. This created very different conditions from before, mainly due to decreased heat transfer from heat blocks to reaction, but also due to

high temperature volatility. Batch no. 4 was because of these factors carried out at too low temperatures, which explains why no CdS cores at all could be detected.

The shortcomings in reaction temperature monitoring lead to yet another modification of the experimental setup. For this final synthesis attempt, the thermometer was inserted into the reaction mixture itself. It was done so by piercing it through one of the septums on the three-necked bottle, see Figure 4.4. The temperature control was greatly enhanced and the volatility altogether disappeared. Instead, issues with achieving sufficient vacuum was introduced as the thermometer compromised the sealing. This approach did however show great promise as the sealing issue is possible to overcome with further small modifications. It is incredibly important to control the exact temperatures, as the tuning of NP size greatly depends on both the exact temperatures but also the times used during synthesis.

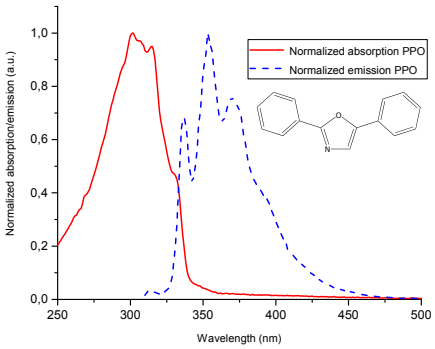


FIGURE 4.4: A snapshot of the CdS/ZnS mixture during the synthesis of batch no. 5. Its vivid yellow color is a result of strong absorption of light in the blue and UV part of the spectrum. To the right one can see the thermometer stick that is inserted through a septum on one of the bottlenecks into the reaction mixture itself.

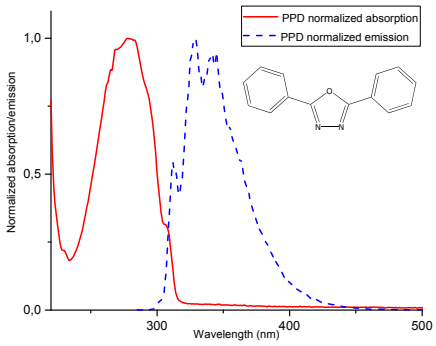
Even though big steps towards attaining proper temperature control of the reaction were made, issues with controlling the amounts of participating compounds remain. Prior to ZnS shell growth, the zinc precursor $Zn(DTTC)_2$ is dissolved in oleylamine. The solubility of $Zn(DTTC)_2$ is however quite low, thus sonication of the solution is needed. Even when sonicated there were severe amounts of precursor falling to the bottom of the solution, thus making it very hard to control the exact amounts that was extracted and subsequently injected into the mixture. Small deviations from the calculated amounts for each ML (see Appendix A.1) will provide disturbances in the shell growth, e.g. by incomplete MLs.

4.2 Annihilator characterization

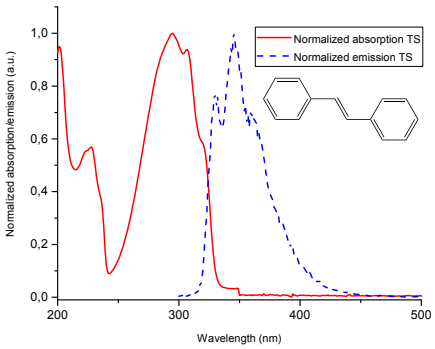
Even though the calculations presented in Figure 2.5 give good indications of where the different energy levels of the prospective annihilators lie, spectroscopic measurements of these compounds were carried out to examine their characteristics. The results of the steady-state absorption and emission measurements done on these compounds are presented in Figure 4.5.



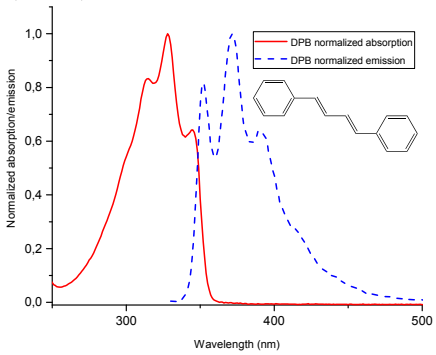
(A) 2,5-diphenyloxazole (PPO)



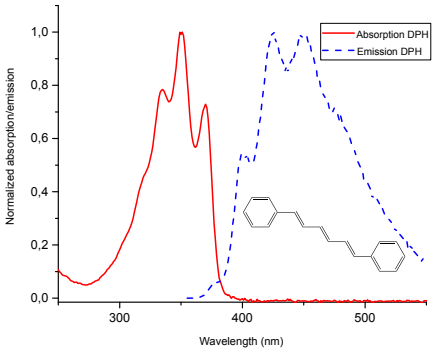
(B) 2,5-diphenyl-1,3,4-oxadiazole (PPD)



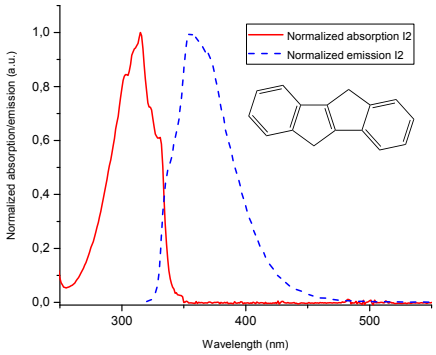
(C) Trans-stilbene (TS)



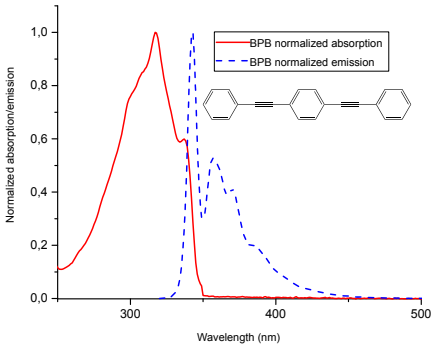
(D) 1,4-diphenyl-1,3-butadiene (DPB)



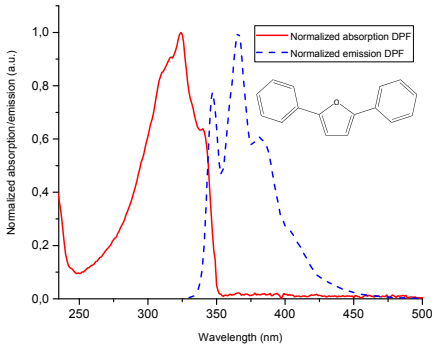
(E) 1,4-diphenyl-1,3,5-hexatriene (DPH)



(F) 5,10-dihydroindeno[2,1-a]indene (I2)



(G) 1,4-bis(phenylethynyl)benzene (BPB)



(H) 2,5-diphenylfuran (DPF)

FIGURE 4.5: Steady-state absorption and emission spectra for the eight annihilator candidates.

The main trend is that the calculated energies from Figure 2.5 are higher than those obtained from the measurements. E.g. DPH, with a calculated S_1 energy of 3.234 eV, should according to the calculations have an emission maximum somewhere around 383 nm, but in reality its emission is centered around 430 nm. This does of course eliminate DPH as a possible annihilator candidate as one requirement is that the annihilator emits in the UV range. The remaining compounds have emission maxima below 400 nm and do as a result fulfill this prerequisite.

4.3 Ligand/mediator exchange investigation

Two of the questions posed in Section 1.3 are related to the two mediators that are investigated in this study: 2,5-diphenyloxazole (PPO) and 2,5-diphenyl-1,3,4-oxadiazole (PPD). In order to answer these a number of different experiments have been performed. Samples with different ratios between NP and mediator concentration were prepared as described in Section 3.2.3.

4.3.1 Measurements on quenching efficiency

First of all the ratio dependence between NPs and mediator was investigated. In Figure 4.6 the absorption and emission spectra for NP:PPO 1:10 and 1:1000 ratios are presented alongside that of pure NPs.

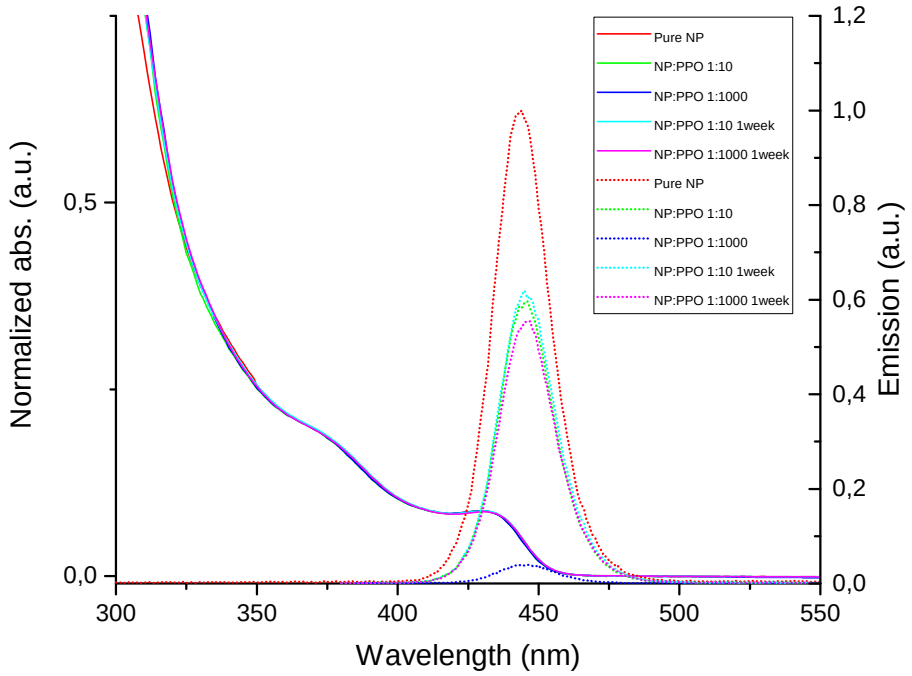


FIGURE 4.6: A series of absorption and emission measurements with PPO as the mediator. The green and light-blue spectra are from measurements on the same sample, with the "1week" notion indicating that the light-blue measurement was performed one week after the green one. The same goes for the blue/purple spectra.

The photoluminescence QY of the NPs has previously been discussed as a high

QY will enhance TET efficiency from NP to mediator. Successful TET, which can only occur if mediator molecules has indeed bound to the surface of the NPs, will in this kind of measurement manifest itself by severe quenching of the NP emission.[26] The amount of quenching is determined by using Equation 3.3. Using PPO as the mediator, the general trend is that the NP emission is quenched by circa 40%. Similar measurements are presented in Figure 4.7. Here, PPD is utilized as mediator instead and NP emission quenching of circa 50% appears, indicating that PPD do bind to a somewhat larger extent than PPO does. As the binding between the mediator is expected to appear between the NP zinc sites and the nitrogen atoms of the mediators, this result is ascribed to PPD having an extra nitrogen atom in the furan ring.

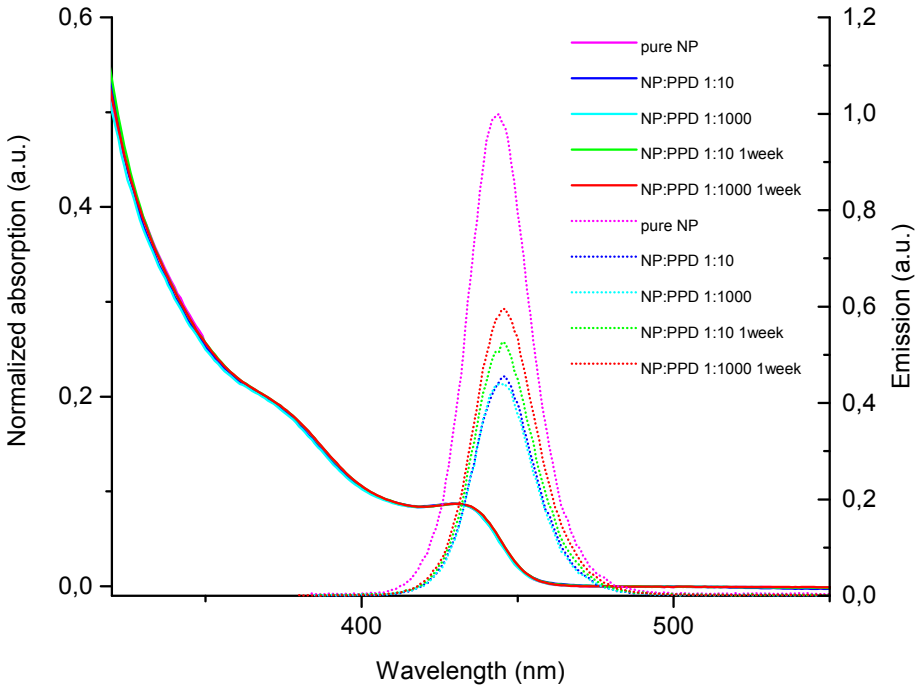


FIGURE 4.7: A series of absorption and emission measurements with PPD as the mediator. The NP emission is quenched by about 50% as PPD binds to the surface.

The blue dotted line in Figure 4.6 diverge from the general trend of the NP/PPO measurements. This specific measurement indicates quenching $> 90\%$ and would if true mean that the TET to the attached PPO mediator is very efficient. Quenching of more than 90% has been produced before by attaching mediators to NP surfaces,[15,26] but as the other measurements in this study all showed substantially lower quenching this measurement had to be considered faulty. This faultiness is further emphasized when compared to the light blue, dotted line in Figure 4.6. This is a measurement on the same sample performed one week later. The discrepancy between the two measurements can only arise for two reasons: either the NP/mediator system is unstable over time, or one of the measurements is faulty. The other samples do not show signs of system instability as the emission is almost identical when measured one week later.

4.3.2 Quantifying the number of surface bound mediators

Efforts in trying to quantify the actual number of PPO/PPD that bound to the NP surface were performed using absorption spectroscopy. The goal was to distinguish the mediator absorption profile from that of the NP, and by comparing their respective absorption be able to quantify the number of molecules attached to the NP surface. This quantification has previously been done successfully by Mongin *et al.* for a system where two carboxylic ligand molecules attached to the surface of cadmium selenide (CdSe) NPs.[26] In their study the absorptive characteristics of the carboxylics were clearly visible and they could, using the molar extinction coefficients (ε) of the participating compounds, conclude that circa 12 molecules attached to each CdSe NP.

For the systems investigated in this study it was soon realized that this method, unfortunately, couldn't be applied. Figure 4.8 illustrates why this is. The four lines show the absorption of four different solutions: one with pure NPs, and three where the amount of PPO is risen by a factor of 10 each time. These samples have *not* been cleaned following the addition of PPO, meaning that the ratios presented are exact.

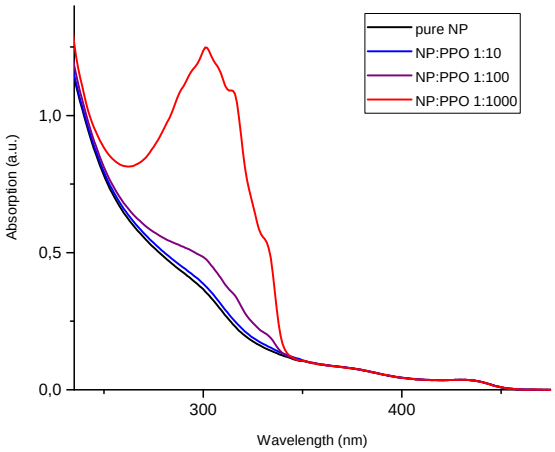


FIGURE 4.8: Absorption of NP/PPO systems of three different ratios, together with the absorption of pure NPs. The PPO feature is only clearly visible for the sample with a 1:1000 NP:PPO ratio. Note that these samples have *not* been cleaned following the addition of PPO.

It is clearly visible that even for the solution with a 1:100 NP:PPO ratio it is quite hard to distinguish the PPO absorption features, and more or less impossible for the 1:10 sample. The reason to why these features are only visible at higher PPO concentrations is related to the molar extinction coefficient, ε, of the NPs and of PPO. Yu *et al.* has experimentally determined how ε for CdSe, CdTe, and CdS NPs may be calculated from their respective absorption spectra.[33] The equations for CdSe and CdS NPs are given by Equations 4.2a and 4.2b:

$$\varepsilon_{CdSe} = 1600\ \Delta E\ (D)^3 \tag{4.2a}$$

$$\varepsilon_{CdS} = 5500\ \Delta E\ (D)^{2.5} \tag{4.2b}$$

where ΔE is the transition energy of the first absorption peak given in eV, and D is the NP diameter in nm. Mongin *et al.*[26] synthesized CdSe NPs with ε_{CdSe} = 59 200 M^{-1} cm^{-1}, which is on the same order as ε of many molecular chromophores, e.g. PPO (ε_{PPO} = 35 700 M^{-1} cm^{-1} at 303 nm). This value is however order of magnitudes larger for CdS NPs, and estimates based on Equation 4.2b give $\varepsilon_{CdS/ZnS}$ = 662 700 M^{-1} cm^{-1} at 430 nm. There is of course an error in this value as the calculation is for only the CdS core, but the sizeable difference to ε_{PPO} holds true.

In fact, considering the TEM image of Figure 4.1, $\varepsilon_{CdS/ZnS}$ might be even higher as the NPs are a bit larger than expected. No matter what, $\varepsilon_{CdS/ZnS}$ will be several times higher at 303 nm as the CdS/ZnS NPs absorb even stronger in the UV regime (see e.g. the absorption spectra in Figure 4.8). As a result, the CdS/ZnS NPs absorb at least two orders of magnitude stronger than PPO at 303 nm, which goes well together with the results presented in Figure 4.8. Figures 4.6 and 4.7 show no pronounced difference in absorption between the 1:10 and 1:1000 NP:PPO/PPD samples, indicating that the number of mediators on each molecule is below 10 after washing. Their respective absorption spectra also indicates that quite few mediators are attached, as no mediator absorption profile is visible.

4.4 Upconversion measurements

The ultimate goal of all the different experiments that has been carried out is of course to try and achieve sTTA-UC in the end. Even though the sensitizer quality and subsequent TET efficiency to the mediators isn't as high as in previous studies, sTTA-UC has indeed been realized.

4.4.1 Effect on UC by change of mediator

Figure 4.9 shows the UC for a system excited with 405 nm light, where PPO acts as both mediator and annihilator. A clear emission signal ranging from 330 nm to 370 nm is visible, and is attributed to UC. This was verified by repeating the same measurement (again using $\lambda_{exc} = 405$ nm) on a sample with only PPO. This sample showed no emission below 370 nm, thus any emission occurring in that range must be the result of UC. The emission that appears in the range between 410 nm and 480 nm is the result of CdS/ZnS emission. Emission in the 370 to 410 nm range and above 480 nm is from scattering of the light source. The gap from 405 nm to 450 nm is the result of over-saturation in the detector, and in reality the emission in this energy range is higher than 16 000 arbitrary units (a.u.). The signature that appears just below 600 nm is an artifact of the 405 nm LED lamp used for the UC measurements, and was present also when only scattering the light through an empty cuvette. The narrow peak at 343 nm is an artifact of the spectrometer and was present even when the sample holder was empty.

On the left-hand side the upconverted emission is compared to the emission profile of free PPO in hexane (the solid, blue line). The main 355 nm peak is prominent, but the higher energy peak, centered at around 335 nm, do not appear in the upconverted spectra. This is probably due to the CdS/ZnS sensitizer absorbing strongly in the deeper UV region. The upconverted photons are reabsorbed by the NPs and does therefore not reach the detector. This phenomenon is called the *inner filter effect*[18] and will severely inhibit detectable UC emission. This is one of the reasons behind that the UC QY, Φ_{UC}, is far below one percent for this sample.

The system with CdS/ZnS as sensitizer and PPO as mediator and annihilator, has previously produced UC emission with better results.[15] In the present study it is also showed that PPD might be used as the mediator compound. In Figure 4.10

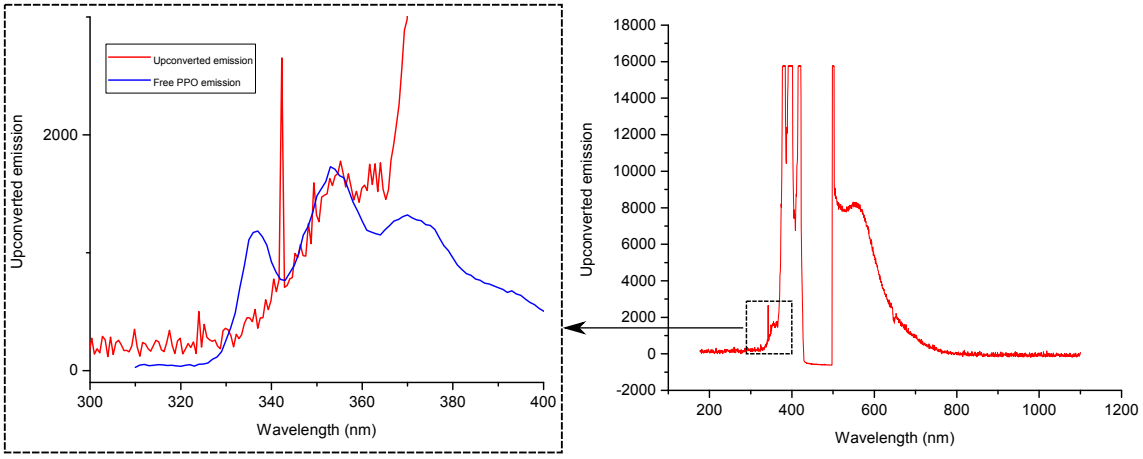


FIGURE 4.9: The recorded emission from a sample where PPO is utilized as both mediator and annihilator. Upconverted emission from PPO is clearly distinguishable under 405 nm excitation light. The UC emission is centered around 355 nm which is the emission maxima for PPO in hexane (blue solid line).

upconverted emission of a system with PPD as mediator and PPO as annihilator is plotted alongside that of when PPO is the mediator.

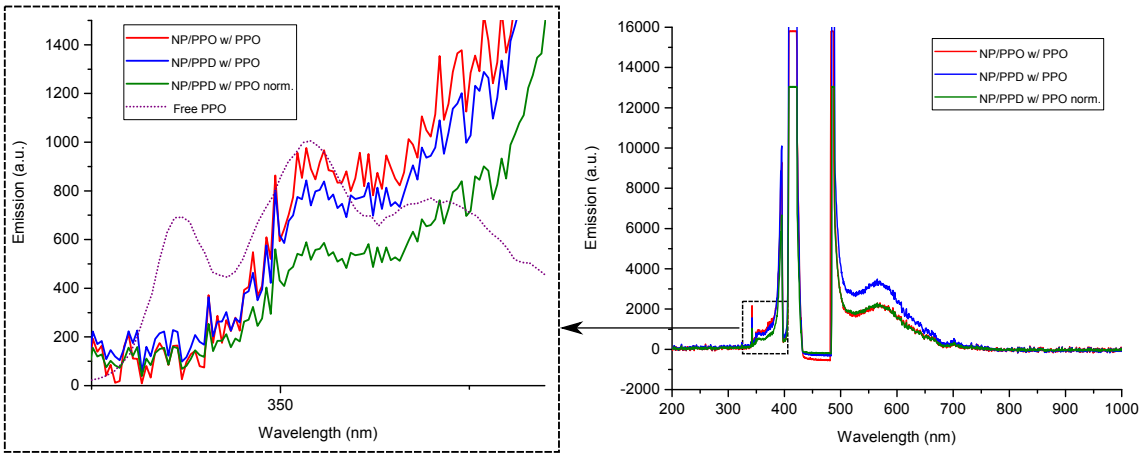


FIGURE 4.10: Upconverted emission from two different samples under 405 nm excitation light: one with PPO as mediator (red line) and one with PPD as mediator (blue line). The green line is the blue spectra normalized with respect to the 570 nm peak to match that of the red one. Both samples utilized PPO as annihilator.

The blue line is the emission of the sample using PPD as the mediator. Using the broad, low energy peak originating from the LED, this spectra could be normalized and compared with the emission from the sample utilizing PPO as mediator. This was needed since the experimental setup was very sensitive to even tiny disturbances. The intensity, and resulting outgoing emission, was because of this hard to keep at a constant rate. However, this clever way of normalizing enables relative comparison betwen the upconverted emissions. From this it is clearly seen that using PPD as the mediator give circa 40% less UC.

Based on the ligand/mediator exchange measurements from Section 4.3.1 this

might be slightly surprising. Considering that the same annihilator is used for both samples, it could be argued that the UC emission should only be proportional to the quenching of the NP emission. If this is the case, the use of PPD as mediator should result in a slightly higher UC than if PPO is used as mediator, as higher quenching indicates more efficient TET. The TET efficiency, Φ_{TET}, is in turn one of the terms for calculating the UC QY, Φ_{UC} (see Equation 2.11).

One possible explanation to this result is that the PPD *doesn't* actually act as mediator. Since PPO is the annihilator, these molecules might bind to the NPs as these are added to the mixture. The annihilator concentration is very high ([A] = 5.7×10^{-3} M) and as it has also been shown that PPO may act as mediator, it could in fact take on that role even in the presence of PPD. Becuase of PPD molecules already being attached to NPs, less PPO may bind in than would have been possible if PPD were absent. This would result in less UC for this sample than for the one where only PPO is present alongside the NPs, which is what we see. If this hypothesis holds true it would mean that the TET from the NPs to the PPO annihilator is hindered somewhere along the way. Considering that the triplet energy of PPD lies very close to that of the NPs, a possible energy mismatch between these might be causing problems. PPD could simply have a too high triplet energy level to allow efficient TET from the NPs, thus not mediating the energy transfer as well as PPO does. Further studies, where e.g. the NP size is altered, would bring insight to this matter.

4.4.2 Novel annihilator UC measurements

Apart from PPO, seven other compounds were tested as annihilators. Unfortunately, the measurements showed no detectable UC emission from any of these other compounds. The findings from the UC measurements are summarized in Table 4.2.

Table 4.2: Summary of the results from the UC measurements. PPO is the only compound that was successfully utilized in the role of annihilator, producing upconverted emission in the 340 nm to 370 nm wavelength range.

Anni. / Med.	PPO	PPD	TS	DPB	DPH	I2	BPB	DPF
PPO	UC	No UC	No UC	No UC	No UC	No UC	No UC	No UC
PPD	UC	No UC	No UC	No UC	No UC	No UC	No UC	No UC

Figure 4.11 illustrates three measurements, using DPB and DPH as annihilators, where no UC was detected. The same emission profile in the UV part of the spectrum was observed for all annihilators except for PPO.

UC wasn't expected from the DPH sample due to its blue emission and sub-optimal energy levels. The remaining compounds could have, based on the initial characterization, participated successfully for TTA but doesn't appear to have done so. It is hard to determine exactly what step has been the limiting one based on only the measurements performed in this study. It has previously been concluded

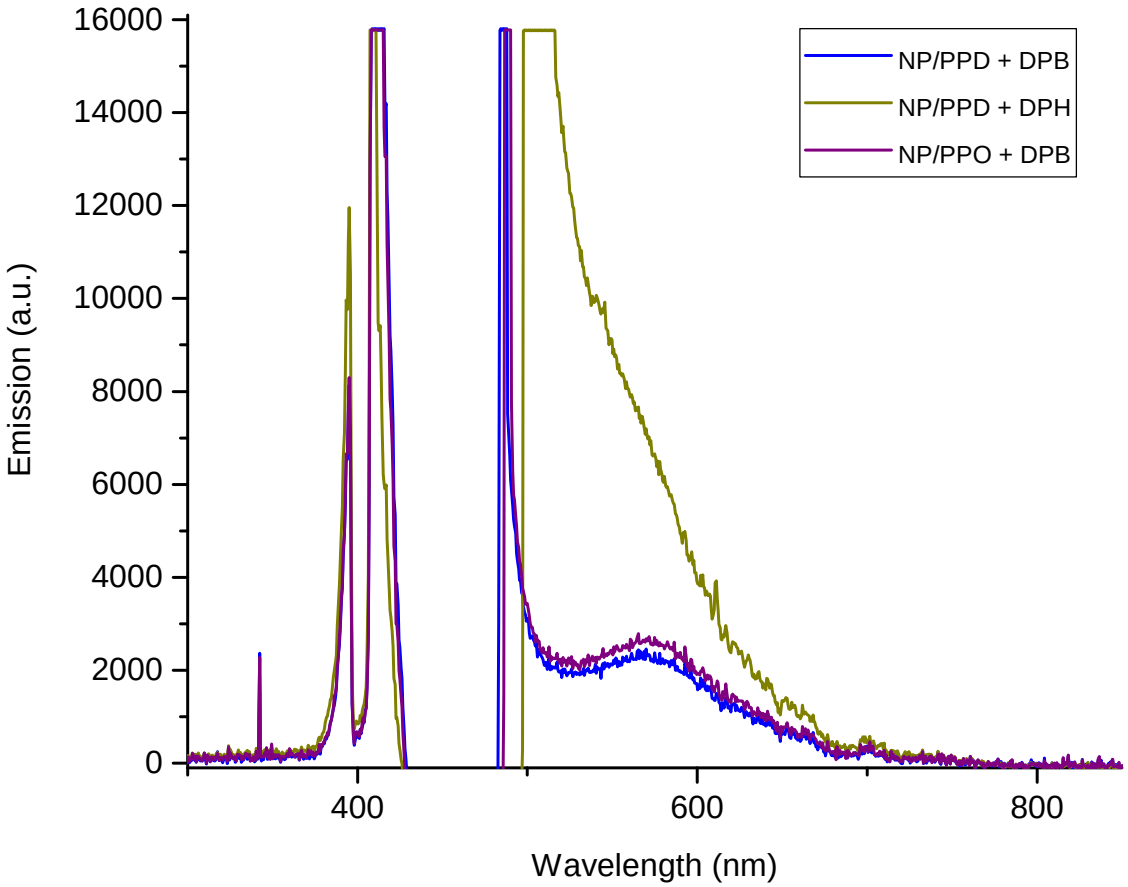


FIGURE 4.11: UC measurements on three different samples, using DPB and DPH as annihilators. DPH emits at too low energies to actually enable UC. If DPB would have been emitting, this should present itself in the form of emission around 360 nm.

that the TTA QY, Φ_{TTA}, is the limiting factor when PPO is used for annihilation.[15] Considering that most of the tested compounds in this study have triplet energy levels below that of PPO (see Figure 2.5) efficient TET should be possible, given that the annihilator concentration is high enough. The absence of UC emission is for this reason primarily ascribed to low Φ_{TTA}. For a few compounds, namely DPB, DPH, and BPB, poor solubility in hexane proved to be an issue. This resulted in lower concentrations for these compounds, and should provide an obstacle for both efficient TET and TTA, given that these processes are dependent on diffusion facilitated collisions between compounds.

4.4.3 Future directions in vis-to-UV UC research

The results of this study further emphasizes what has previously been realized - achieving vis-to-UV UC is very tricky. No new annihilators has been added to the list of compounds that actually work, but understanding *why* they don't work remains rather uncertain. These compounds might however not be solely responsible for the absence of UC, considering that the sensitizer and experimental setup is suboptimal. Continued efforts to try and synthesize higher quality CdS/ZnS NPs

must be done in order to give new annihilator candidates better requisites. An even more important factor is the experimental setup, as the utilization of LED light is far inferior to that of laser light. Using an external power supply meant that the resulting intensity couldn't be monitored as the UC measurements were ongoing, but instead an estimate was used based on the spot size at the sample and the premeasured effect of incident light. Estimates gave that the resulting maximum incident intensity was around 500 mW/cm^2. A previous study utilizing PPO as annihilator[15] has stated that the threshold intensity, I_{th}, lie at 7 W/cm^2 which is more than one magnitude higher than the intensities that could be realized in this study.

For this reason it is not surprising that recorded UC emission here is very low or non-existent, even though there also must be other, intrinsic properties of these molecules that hinder successful sTTA-UC. More sophisticated spectroscopy techniques must be utilized to gain understanding of the underlying mechanisms. The Jablonski diagram in Figure 2.1 mentions *excited state absorption*, a phenomenon among others that can be investigated using *transient absorption spectroscopy*.[18] This is a technique that measures how the absorbance of a sample changes over time after excitation. Usually these changes appear on very short timescales (μs, 10^{-6}, down to fs, 10^{-15}) and by analyzing how the spectra changes, information about what processes are ongoing in the system may be obtained. Signatures of absorption between triplet states not visible using regular absorption spectroscopy could for instance be visualized. The presence of such signals in these samples would indicate that TET has in fact been realized from NPs to annihilator.[15]

5
Conclusion

In this study the mechanisms behind sTTA-UC from vis-to-UV has been investigated. The CdS/ZnS core-shell NP sensitizer was successfully synthesized and utilized for sTTA-UC. These particles displayed a photoluminescence QY, Φ_{PL}, of 7.3 $\pm$ 0.3%, which was enough to achieve UC. There are however room for severe improvements to be done on the NP quality, something that would enhance the resulting Φ_{UC}. A number of different compounds were for the first time tested in the role as annihilator. These results indicates that none of the novel compounds displayed any UC emission, however UC occurred when the previously used fluorophore 2,5-diphenyloxazole (PPO) acted as annihilator. Even though the Φ_{UC} was far below one percent, this stands as an important proof of concept of vis-to-UV UC in solution. Two different mediator compounds were tested, and both PPO and 2,5-diphenyl-1,3,4-oxadiazole (PPD) was successfully implemented in this role. Quenching of the NP emission, resulting from the mediator compounds binding to the NP surface, indicated that TET was slightly more effective from NP to PPD than to PPO. UC measurements however showed that a higher Φ_{UC} could be reached when PPO acted as mediator. This raises questions whether PPD actually acts as the mediator or if PPO take on both roles of mediator and annihilator even in the presence of PPD. More experiments need to be designed in order to answer such questions, and also to increase the understanding of why the novel compounds are seemingly non-functioning as annihilators.

5.1 Future outlook

Even when the sensitizer has been of high quality, the highest achieved Φ_{UC} of 2.6% for vis-to-UV UC is relatively low.[15] Because of this it is of utmost importance to further improve the synthesis of the CdS/ZnS NP sensitizer. Only when the very highest sensitizer quality is assured may accurate conclusions regarding other aspects of the upconverting system be made. Continued efforts in optimizing current synthesis routes as well as developing new methods will be crucial in order to develop NP sTTA-UC. In addition to this, a more thorough investigation on why PPO may perform TTA must be undertaken. Trying to predict which compounds may be used as annihilators based on e.g. energy calculations is of course necessary, but without a deeper understanding on why e.g. PPO actually works, such efforts may be a waste of time. Transient absorption should be utilized to monitor the ongoing processes in both functioning sTTA-UC systems with PPO, as well as in non-functioning systems. It must also be investigated how current sTTA-UC systems may be realized in the

solid state, as this will be a requirement for future implementations. Continuous efforts into the examination of new possible sensitizer, mediator, and annihilator compounds must also be performed.

Bibliography

[1] M. Gratzel, "Photoelectrochemical Cells", *Nature*, vol. 414, no. 6861, pp. 338–344, 1995.

[2] M. A. Green, Y. Hishikawa, W. Warta, E. D. Dunlop, D. H. Levi, J. Hohl-Ebinger, and A. W. Ho-Baillie, "Solar cell efficiency tables (version 50)", *Progress in Photovoltaics: Research and Applications*, 2017.

[3] N. Menyuk, K. Dwight, and J. W. Pierce, "NaYF 4 : Yb,Er—an efficient up-conversion phosphor Application of up-converting phosphors for enhanced near-infrared silicon solar cell response New transparent vitroceramics codoped with Er 3+ and Yb 3+ for efficient frequency upconversion NaYF 4 : Yb,Er-", *Applied Physics Letters*, vol. 21, no. 10, 1972.

[4] S. Hoseinkhani, R. Tubino, F. Meinardi, and A. Monguzzi, "Achieving the photon up-conversion thermodynamic yield upper limit by sensitized triplet–triplet annihilation", *Phys. Chem. Chem. Phys.*, 2015.

[5] V. Gray, D. Dzebo, M. Abrahamsson, B. Albinsson, and K. Moth-Poulsen, "Triplet–triplet annihilation photon-upconversion: towards solar energy applications", *Phys. Chem. Chem. Phys.*, 2014.

[6] A. J. Bard and M. A. Fox, "Hydrogen and Oxygen", *Acc. Chem. Res*, vol. 28, pp. 141–145, 1995.

[7] F. Rizzi, E. Annunziata, G. Liberati, and M. Frey, "Technological trajectories in the automotive industry: are hydrogen technologies still a possibility?", *Journal of Cleaner Production*, vol. 66, pp. 328–336, 2014.

[8] P. Nikolaidis and A. Poullikkas, "A comparative overview of hydrogen production processes", *Renewable and sustainable energy reviews*, vol. 67, pp. 597 – 611, 2016.

[9] H. Kato, K. Asakura, and A. Kudo, "Highly Efficient Water Splitting into H 2 and O 2 over Lanthanum-Doped NaTaO 3 Photocatalysts with High Crystallinity and Surface Nanostructure", *J. Am. Chem. Soc.*, vol. 125, pp. 3082–3089, 2003.

[10] C. A. Parker and T. A. Joyce, "Phosphorescence of Benzophenone in Fluid Solution", *Chemical Communications*, no. 13, pp. 749–750, 1968.

[11] G. Bergamini, P. Ceroni, M. Maestri, V. Balzani, S.-K. Lee, and F. Vögtle, "Forward (singlet–singlet) and backward (triplet–triplet) energy transfer in a dendrimer with peripheral naphthalene units and a benzophenone core", *Photochemical & photobiological sciences : Official journal of the European Photochemistry Association and the European Society for Photobiology*, vol. 3, no. 9, pp. 898–905, 2004.

[12] T. N. Singh-Rachford and F. N. Castellano, "Photon upconversion based on sensitized triplet-triplet annihilation", *Coordination Chemistry Reviews*, 2010.

[13] P. Duan, N. Yanai, and N. Kimizuka, "A bis-cyclometalated iridium complex as a benchmark sensitizer for efficient visible-to-uv photon upconversion", *Chemical Communications*, vol. 50, no. 86, pp. 13 111–13 113, 2014.

[14] N. Yanai, M. Kozue, S. Amemori, R. Kabe, C. Adachi, and N. Kimizuka, "Increased vis-to-UV upconversion performance by energy level matching between a TADF donor and high triplet energy acceptors", *J. Mater. Chem. C*, vol. 4, no. 27, pp. 6447–6451, 2016.

[15] V. Gray, P. Xia, Z. Huang, E. Moses, A. Fast, D. A. Fishman, V. I. Vullev, M. Abrahamsson, K. Moth-Poulsen, and M. L. Tang, "CdS/ZnS core–shell nanocrystal photosensitizers for visible to UV upconversion", *Chemical Science*, vol. 8, no. 8, 2017.

[16] P. B. Merkel and J. P. Dinnocenzo, "Low-power green-to-blue and blue-to-UV upconversion in rigid polymer films", *Journal of Luminescence*, vol. 129, no. 3, pp. 303–306, 2009.

[17] W. Thatcher Borden, R. Hoffmann, T. Stuyver, and B. Chen, "Dioxygen: What Makes This Triplet Diradical Kinetically Persistent?", *Journal of the American Chemical Society*, vol. 139, no. 26, pp. 9010–9018, 2017.

[18] J. R. Lakowicz, *Principles of Fluorescence Spectroscopy*, 3rd ed. Springer, 2006.

[19] O. Gijzeman, F. Kaufman, and G. Porter, "Oxygen quenching of aromatic triplet states in solution. Part 1", *Journal of the Chemical Society, Faraday Transactions 2: Molecular and Chemical Physics*, vol. 69, pp. 708–720, 1973.

[20] B. Albinsson, M. P. Eng, K. Pettersson, and M. U. Winters, "Electron and energy transfer in donor–acceptor systems with conjugated molecular bridges", *Physical Chemistry Chemical Physics*, vol. 9, no. 44, pp. 5847 – 5864, 2007.

[21] D. Y. Kondakov, T. D. Pawlik, T. K. Hatwar, and J. P. Spindler, "Triplet annihilation exceeding spin statistical limit in highly efficient fluorescent organic light-emitting diodes", *Journal of Applied Physics*, vol. 106, 2009.

[22] Y. Y. Cheng, B. Fückel, T. Khoury, C. G. C. R. Raphaël, M. J. Y. Tayebjee, N. J. Ekins-Daukes, M. J. Crossley, and T. W. Schmidt, "Kinetic Analysis of Photochemical Upconversion by Triplet-Triplet Annihilation: Beyond Any Spin Statistical Limit", *J. Phys. Chem. Lett*, vol. 1, pp. 1795–1799, 2010.

[23] A. Monguzzi, J. Mezyk, F. Scotognella, R. Tubino, and F. Meinardi, "Upconversion-induced fluorescence in multicomponent systems: Steady-state excitation power threshold", *Physical Review B*, vol. 78, no. 19, 2008.

[24] V. Gray, "Synthesis and Photophysical Characterization of Annihilator- Sensitizer Pairs for Triplet-Triplet Annihilation Based Photon Upconversion", Chalmers University of Technology, Gothenburg, Tech. Rep., 2017.

[25] Z. Huang, X. Li, M. Mahboub, K. M. Hanson, V. M. Nichols, H. Le, M. L. Tang, and C. J. Bardeen, "Hybrid molecule–nanocrystal photon upconversion across the visible and near-infrared", *Nano letters*, vol. 15, no. 8, pp. 5552–5557, 2015.

[26] C. Mongin, S. Garakyaraghi, N. Razgoniaeva, M. Zamkov, and F. N. Castellano, "Direct observation of triplet energy transfer from semiconductor nanocrystals", *Science*, vol. 351, no. 6271, pp. 369–372, 2016.

[27] K. Okumura, K. Mase, N. Yanai, and N. Kimizuka, "Employing Core-Shell Quantum Dots as Triplet Sensitizers for Photon Upconversion", *Chemistry - A European Journal*, vol. 22, no. 23, pp. 7721–7726, 2016.

[28] G. D. Scholes, "Controlling the optical properties of inorganic nanoparticles", *Advanced Functional Materials*, vol. 18, no. 8, pp. 1157–1172, 2008.

[29] C. De Mello Donegá and R. Koole, "Size Dependence of the Spontaneous Emission Rate and Absorption Cross Section of CdSe and CdTe Quantum Dots", *Journal of Physical Chemistry*, vol. 113, no. 16, 2009.

[30] L. Brus, "Electronic Wave Functions in Semiconductor Clusters: Experiment and Theory", *J. Phys. Chem*, vol. 90, pp. 2555–2560, 1986.

[31] D. Chen, F. Zhao, H. Qi, M. Rutherford, and X. Peng, "Bright and stable purple/blue emitting CdS/ZnS Core/Shell nanocrystals grown by thermal cycling using a single-source precursor", *Chemistry of Materials*, vol. 22, no. 4, pp. 1437–1444, 2010.

[32] Zou, R. B. Little, J. P. Wang, and M. A. El-Sayed, "Effect of different capping environments on the optical properties of CdS nanoparticles in reverse micelles", *International Journal of Quantum Chemistry*, vol. 72, pp. 439–450, 1999.

[33] W. W. Yu, L. Qu, W. Guo, and X. Peng, "Experimental Determination of the Extinction Coefficient of CdTe, CdSe, and CdS Nanocrystals", *Chemistry of Materials*, vol. 15, no. 14, pp. 2854–2860, 2003.

[34] C. M. Marian, "Spin-orbit coupling and intersystem crossing in molecules", *Wiley Interdisciplinary Reviews: Computational Molecular Science*, vol. 2, no. 2, pp. 187–203, 2012.

[35] H. Zhu, N. Song, and T. Lian, "Controlling Charge Separation and Recombination Rates in CdSe/ZnS Type I Core-Shell Quantum Dots by Shell Thicknesses",

Journal of the American Chemical Society, vol. 132, no. 42, pp. 15 038–15 045, 2010.

[36] B. Steyer and F. P. Schfifer, "Applied Physics Stimulated and Spontaneous Emission from Laser Dyes in the Vapor Phase", *Applied physics*, vol. 7, no. 1, pp. 3–122, 1975.

[37] D. G. Whitten, "Photochemistry and Photophysics of trans-Stilbene and Related Alkenes in Surfactant Assemblies", *Acc. Chem. Res*, vol. 26, pp. 502–509, 1993.

[38] D. C. Todd, J. M. Jean, S. J. Rosenthal, A. J. Ruggiero, D. Yang, and G. R. Fleming, "Fluorescence upconversion study of cis-stilbene isomerization", *The Journal of Chemical Physics*, vol. 931, no. 10, 1990.

[39] J. Saltiel, O. C. Zafiriou, E. D. Megarity, and A. A. Lamola, "Tests of the Singlet Mechanism for cis-trans Photoisomerization of the Stilbenes", *Journal of the American Chemical Society*, vol. 90, no. 17, pp. 4759–4760, 1968.

[40] M. Biswas, P. Nguyen, T. B. Marder, and L. R. Khundkar, "Unusual Size Dependence of Nonradiative Charge Recombination Rates in Acetylene-Bridged Compounds", *The Journal of Physical Chemistry A*, vol. 101, no. 9, pp. 1689–1695, 1997.

[41] T. N. Singh-Rachford and F. N. Castellano, "Low power visible-to-UV upconversion", *Journal of Physical Chemistry A*, 2009.

[42] M. Sumitani, N. Nakashima, K. Yoshihaju, and S. Nagakura, "Temperature dependence of fluorescence lifetimes of trans-stilbene", *Chemical Physics Letters*, vol. 51, no. 1, pp. 183–185, 1977.

[43] J. F. Pfanstiel, B. B. Champagne, W. A. Majewski, D. F. Plusquellic, and D. W. Pratt, "A Rotationally Resolved Fluorescence Excitation Spectrum of all-trans-1,4-diphenyl-1,3", *Science*, vol. 245, no. 18, pp. 736–738, 1989.

[44] E. D. Cehelnik, R. B. Cundall, J. R. Lockwood, and F. T. Palmer, "Solvent and Temperature Effects on the Fluorescence of all-trans- 1,6-Diphenyl-1,3,5-hexatriene", *The Journal of Physical Chemistry*, vol. 79, no. 14, pp. 1369–1376, 1975.

[45] M. Levitus, K. Schmieder, H. Ricks, K. D. Shimizu, U. H. Bunz, and M. A. Garcia-Garibay, "Steps to demarcate the effects of chromophore aggregation and planarization in poly(phenyleneethynylene)s. 1. Rotationally interrupted conjugation in the excited states of 1,4-bis(phenylethynyl)benzene", *Journal of the American Chemical Society*, vol. 123, no. 18, pp. 4259–4265, 2001.

[46] M. Oelgemöller, B. Brem, R. Frank, S. Schneider, D. Lenoir, N. Hertkorn, Y. Origane, P. Lemmen, J. Lex, and Y. Inoue, "Cyclic trans-stilbenes: synthesis, structural and spectroscopic characterization, photophysical and photochemical properties", *Journal of the Chemical Society, Perkin Transactions 2*, no. 10, pp. 1760–1771, 2002.

[47] G. Heinrich, S. Schoof, and H. Gusten, "9,10-diphenylanthracene as a fluorescence quantum yield standard", *Journal of Photochemistry Elsevier Sequoia S.A*, vol. 3, pp. 315–320, 1974.

[48] J. V. Morris, M. A. Mahaney, and J. R. Huber, "Fluorescence Quantum Yield Determinations. 9,10-Diphenylanthracene as a Reference Standard in Different Solvents", *The Journal of Physical Chemistry*, vol. 80, no. 9, pp. 969–974, 1976.

[49] R. R. Islangulov, D. V. Kozlov, and F. N. Castellano, "Low power upconversion using MLCT sensitizers", *Chemical Communications*, no. 30, pp. 3776–3778, 2005.

[50] S. Baluschev, T. Miteva, V. Yakutkin, G. Nelles, A. Yasuda, and G. Wegner, "Up-Conversion Fluorescence: Noncoherent Excitation by Sunlight", *Physical Review Letters*, vol. 97, no. 14, 2006.

[51] R. S. Khnayzer, J. Blumhoff, J. A. Harrington, A. Haefele, F. Deng, and F. N. Castellano, "Upconversion-powered photoelectrochemistry", *Chem. Commun. Chem. Commun*, vol. 48, no. 48, pp. 209–211, 2012.

[52] Z. Li, Y. Ji, R. Xie, S. Y. Grisham, and X. Peng, "Correlation of CdS nanocrystal formation with elemental sulfur activation and its implication in synthetic development", *Journal of the American Chemical Society*, vol. 133, no. 43, pp. 17 248–17 256, 2011.

[53] X. Peng, M. C. Schlamp, A. V. Kadavanich, and A. P. Alivisatos, "Epitaxial Growth of Highly Luminescent CdSe/CdS Core/Shell Nanocrystals with Photostability and Electronic Accessibility", *Journal of the American Chemical Society*, vol. 119, no. 30, pp. 7019–7029, 1997.

[54] A. Veamatahau, B. Jiang, T. Seifert, S. Makuta, K. Latham, M. Kanehara, T. Teranishi, and Y. Tachibana, "Origin of surface trap states in CdS quantum dots: relationship between size dependent photoluminescence and sulfur vacancy trap states", *Phys. Chem. Chem. Phys.*, vol. 17, no. 17, pp. 2850–2858, 2015.

A

Appendix 1

A.1 Calculation: Amount of $Zn(DTTC)_2$ needed for ZnS shell growth

The procedure for calculating the amount of zinc precursor $Zn(DTTC)_2$ needed for shell growth is based on the method by Chen *et al.*[31]

CdS core size: $d_0 = 3.64$ nm, $r_0 = 3.64/2$ nm $= 1.82$ nm

Amount of CdS particles: $n_1 = 1.875\times10^{-7}$ mol

Two possible crystal configurations for ZnS; *zinc blende* or *wurtzite*.

Zinc blende lattice parameters: $a = 0.5406$ nm
Wurtzite lattice parameters: $a = 0.3814$ nm, $c = 0.6257$ nm

Average thickness d of one monolayer (ML) ZnS:
For *zinc blende*: $d = a\frac{\sqrt{3}}{3} = 0.5406\times\frac{1.732}{3}$ nm $= 0.312$ nm
For *wurtzite*: $d = \frac{c}{2} = \frac{0.6257}{2}$ nm $= 0.313$ nm
$d = 0.31$ nm will be used from here on.

Volume of 1st ML ZnS: $r_0 = 3.64/2$ nm $= 1.82$ nm,
$r_1 = r_0 + d = 1.82 + 0.31$ nm $= 2.13$ nm
$V_1 = \frac{4\pi}{3}(2.13^3 - 1.82^3)$ nm^3 $= 1.52\times10^{-26}$ m^3

Density of ZnS:
For *zinc blende*: $\rho = 4.10\times10^6$ g/m^3
For *wurtzite*: $\rho = 4.09\times10^6$ g/m^3
$\rho = 4.10\times10^6$ g/m^3 will be used from here on.

Mass of 1st ML: $m_1 = V_1 \times \rho = 6.24\times10^{-20}$ g
Amount ZnS needed for 1st ML of one particle:
$n_2 = \frac{m}{M.W.} = 6.40\times10^{-22}$ mol/particle
M.W. = molecular weight = 97.747 g/mol for ZnS

Amount $Zn(DTTC)_2$ precursor needed for 1st ML:

$A_1 = n_1 \times N_A \times n_2 = 7.23{\times}10^{-5}$ mol

2nd ML: $A_2 = A_1 \times \frac{V_2}{V_1} = A_1 \times \dfrac{(r_1+d)^3 - r_1^3}{r_1^3 - r_0^3} = 0.968{\times}10^{-4}$ mol

3rd ML: $A_3 = A_1 \times \frac{V_3}{V_1} = A_1 \times \dfrac{(r_1+2d)^3 - (r_1+d)^3}{r_1^3 - r_0^3} = 1.247{\times}10^{-4}$ mol

4th ML: $A_4 = A_1 \times \frac{V_4}{V_1} = A_1 \times \dfrac{(r_1+3d)^3 - (r_1+2d)^3}{r_1^3 - r_0^3} = 1.563{\times}10^{-4}$ mol